Investigating Carbonyl Compounds above the Amazon Rainforest using PTR-ToF-MS with NO⁺ Chemical Ionization

Akima Ringsdorf[1], Achim Edtbauer[1], Bruna Holanda[2], Christopher Poehlker[2], Marta O. Sá[3], Alessandro Araújo[4], Jürgen Kesselmeier[2], Jos Lelieveld[1,5], Jonathan Williams[1,5]

[1]Department of Atmospheric Chemistry, Max Planck Institute for Chemistry, Mainz, Germany

[2]Department of Multiphase Chemistry, Max Planck Institute for Chemistry, Mainz, Germany

[3]Instituto Nacional de Pesquisas da Amazonia (INPA), Manaus, CEP 69067-375, Brazil

[4]Empresa Brasileira de Pesquisa Agropecuaria (Embrapa) Amazonia Oriental, Belem, CEP 66095-100, Brazil

[5]Climate and Atmosphere Research Center, The Cyprus Institute, 1645 Nicosia, Cyprus

Correspondence to: Jonathan Williams (J.Williams@mpic.de) and Akima Ringsdorf (A.Ringsdorf@mpic.de)

Abstract. The photochemistry of carbonyl compounds significantly influences tropospheric chemical composition by altering the local oxidative capacity, free radical abundance in the upper troposphere, and formation of ozone, PAN, and secondary organic aerosol particles. Carbonyl compounds can be emitted directly from the biosphere into the atmosphere and are formed through photochemical degradation of various precursor compounds. Aldehydes have atmospheric lifetimes of hours to days, in contrast to ketones, which persist for up to several weeks. While standard operating conditions for proton transfer time-of-flight mass spectrometer (PTR-ToF-MS) using H_3O^+ ions are unable to separate aldehydes and ketones, the use of NO^+ reagent ions allows for the differential detection of isomeric carbonyl compounds with a high time resolution. Here we study the temporal (24 h) and vertical (80–325 m) variability of individual carbonyl compounds in the Amazon rainforest atmosphere with respect to their rainforest-specific sources and sinks. We found strong sources of ketones within or just above the canopy (acetone, MEK, and C_5-ketones). A common feature of the carbonyls was nocturnal deposition observed by loss rates, most likely since oxidized volatile organic compounds are rapidly metabolized and utilized by the biosphere. With NO^+ chemical ionization, we show that the dominant carbonyl species include acetone and propanal, which are present at a ratio of 1:10 in the wet–to–dry transition and 1:20 in the dry season.

1   Introduction

On a global scale, tropical forests are regarded as the largest source of biogenic volatile organic compounds (BVOC) for the atmosphere (Guenther, 2013). BVOC comprise multiple compound classes including terpenes, alkenes, alkanes, alcohols, acids, esters, halocarbons, and carbonyls, all emitted as a result of various physiological processes, such as those occurring in plants, soils, etc., and as a function of environmental conditions. The emission quantity and composition vary among plant species, thus given the high biodiversity in tropical forests, the ecosystem composition and developmental stage also need to be considered as clearly demonstrated by Ciccioli et al. (2023). Most of the carbon released as BVOC from the tropical rainforest is in the form of terpenes, including the hemiterpene isoprene (C_5H_8) (Yáñez-Serrano et al., 2015), monoterpenes such as alpha-pinene ($C_{10}H_{16}$) (Zannoni et al., 2020b), and sesquiterpenes such as copaene ($C_{15}H_{24}$) (Yee et al., 2020). In addition, considerable amounts of oxygenated VOC (OVOC) are known to be present in rainforest air, with carbonyl compounds, namely aldehydes and ketones containing the C=O functional group, constituting an important subset of the atmospheric OVOC (Kesselmeier and Staudt, 1999). Direct biogenic emission, biomass burning, and secondary formation, mainly from the oxidation of the aforementioned terpene precursors and photolysis of larger carbonyls, all contribute to the cocktail of carbonyl compounds in the atmosphere (Guenther, 2013; Liu et al., 2022; Mellouki et al., 2015). To understand this cocktail, deposition and uptake by vegetation, i.e., bidirectional exchange, should always be considered as potential contributors (Kesselmeier, 2001; Kesselmeier et al., 1997; Villanueva et al., 2014). The formation of carbonyl species occurs after the oxidation of VOC is initiated by the hydroxyl radical (OH), ozone (O_3), or at nighttime by the nitrate radical (NO_3), and the resulting peroxy radicals (RO_2) react either with nitrogen oxide (NO) (when present) or with other ambient RO_2 or

45 HO$_2$ radicals. In the presence of NO this oxidation chain results in a net production of O$_3$, an important radiatively
46 active oxidant in the Amazon and worldwide (Mellouki et al., 2015; Trebs et al., 2012).

47 The main atmospheric carbonyl sinks are photolysis and oxidation by OH (Atkinson and Arey, 2003). As a
48 consequence, reactions with carbonyls combined with those of other BVOC determine the availability of OH and thus
49 the oxidative capacity of the atmosphere (Lelieveld et al., 2016). In Amazon rainforest air, OVOC account for 22-40 %
50 of OH reactivity, namely the overall loss frequency of OH radicals (Pfannerstill et al., 2021). Unsaturated carbonyls,
51 like the isoprene oxidation products methacrolein (MACR) and methyl vinyl ketone (MVK), are also oxidized by O$_3$.
52 Ketones, such as acetone, react much less readily with OH than aldehydes and, accordingly, have longer atmospheric
53 lifetimes. Thus, they persist during long-range transport and convective lifting to high altitudes, whereas more reactive
54 aldehydes impact the chemistry more locally. However, through rapid, deep convection, a frequent phenomenon in
55 the humid and hot tropics, also aldehydes can be transported to altitudes between 10 and 17 km (Prather and Jacob,
56 1997).

57 Oxidation of aldehydes and photolysis of ketones and dicarbonyls and further reaction with NO$_x$ (NO + NO$_2$) yields
58 peroxycarboxylic nitric anhydride (PAN). PAN and other peroxynitrates are thermally unstable near the surface but
59 in the cooler mid- and upper troposphere PAN is the most abundant reservoir for nitrogen oxides and is transported
60 over long distances (Mellouki et al., 2015; Fischer et al., 2014; Singh et al., 1990; Roberts, 2007). The main precursors
61 of PAN are acetaldehyde, followed by more minor contributions from methylglyoxal (not reported here) and acetone
62 (Fischer et al., 2014). NO$_x$ in the tropical atmosphere originates from several processes, starting with microbial
63 activities in soils and the release of NO, which is rapidly oxidized to NO$_2$, a large fraction even before it escapes the
64 canopy. NO$_2$ can be taken up by vegetation and only a part of this species traverses the canopy to the atmosphere
65 above (Breuninger et al., 2013; Chaparro-Suarez et al., 2011; Rummel et al., 2002). Further sources are lightning
66 discharges and biomass burning, the latter having the strongest seasonal variability (Bond et al., 2002).

67 The photochemical degradation of carbonyls in the atmosphere is also a source of HO$_x$ (HO$_2$ + OH) radicals,
68 particularly important in the upper troposphere where OH radical production from carbonyls can exceed primary
69 production in areas impacted by convection (Colomb et al., 2006; Lary and Shallcross, 2000; Liu et al., 2022; Prather
70 and Jacob, 1997). Furthermore, the abundance of radicals and oxidation products of carbonyls and dicarbonyls can
71 promote the formation and growth of secondary organic aerosols (Liu et al., 2022).

72 In this study, the observed diel and vertical (80-325 m) variability of 15 carbonyl species (C$_2$-C$_9$) was investigated.
73 These species were detected online with a PTR-ToF-MS using NO$^+$ as a reagent ion. This technique enables the
74 separation of isomeric aldehydes and ketones to identify their partitioning in the Amazonian atmospheric boundary
75 layer (ABL) at the ATTO site. Previous measurements of carbonyls have been conducted over the rainforest using
76 PTR-MS with H$_3$O$^+$ as the reagent ion(Yáñez-Serrano et al., 2016). With this method, both aldehyde and ketone
77 carbonyl forms are detected at the same mass. Usually, for airborne measurements, atmospheric chemists have argued
78 that the m/z used for the detection of C$_3$ carbonyls can be interpreted to be predominantly acetone since its atmospheric
79 lifetime is relatively long (Williams et al., 2001). However, near biogenic sources, the fractional distribution can be
80 different, and especially if the data is used to extract further information about the environment, such as OH
81 concentrations (Williams et al., 2000), the validity of this assumption should be verified.

82 The dataset presented here is the first online measurement of speciated individual aldehydes and ketones in the
83 Amazon. This rainforest environment is characterized by high solar insolation and vigorous vertical transport by deep
84 convection. In quantifying the relative abundance of carbonyl species, we aimed to improve the understanding of their
85 emissions, secondary formation in the atmosphere, transformation, and deposition in the Amazon rainforest region.

86 **2   Experimental**

87 **2.1   Measurement site and instrumentation**

88 All measurements were conducted at the Amazon Tall Tower Observatory (ATTO) within the primary tropical
89 rainforest of Brazil. The site is located 135 km NE of Manaus (02.14°S,58.99°W, 120 m above sea level) with the
90 main wind direction being NE to SE (Fig. S1). In the wet season (February–May), the air is typically nearly pristine

91 since the air masses pass over more than 1000 km of mostly unperturbed rainforest before being sampled, with a
92 possible influence due to long-range transport from African biomass burning pollution, which has been observed in
93 the beginning of the dry season (Fabruary–March) (Holanda et al., 2023). This is reflected by low concentrations of
94 NO_x of less than 150 ppt in the ABL during the late wet season. In the dry season (August-November), however, air
95 influenced by mainly man-made biomass burning in South America was observed. In the same season enhanced black
96 carbon concentrations were measured due to the hemispheric wide summer maximum in biomass burning. The site
97 hosts a 325–m–tall tower and an 80–m walk-up tower, among other measurement and accommodation facilities. A
98 detailed map can be found in the Supplement (Fig. S2). The canopy height of the surrounding forest is about 35 m
99 (Kuhn et al., 2007). A comprehensive description of the site is provided by Andreae et al. (2015). The measurements
100 described here were conducted from June 23 until July 8 and from September 27 until October 14, 2019.

101 The sampling inlets for the BVOC measurements are located at 80, 150, and 325 m on the tall tower. Air is drawn by
102 high-volume pumps down to the instrumentation that is stored in an air-conditioned container at the foot of the tower.
103 By sequentially sampling each height for 5 minutes, a semi-continuous measurement can be achieved, so that each
104 height is sampled four times per hour. The flow in the insulated and heated (40 °C) Teflon sampling lines (3/8″OD)
105 is about $10\,l\,min^{-1}$. A long inlet line can be compared to a gas chromatographic column, which retains the sampled
106 VOC depending on their volatility and polarity, expressed by a wall saturation concentration (Pagonis et al., 2017).
107 The flow through the 325 m Teflon line caused a response time of 90 seconds at ATTO using a VOC gas standard.
108 Before the actual sampling of each height, the line was flushed with ambient air to achieve saturation. Tests with a
109 400–m inlet line in China have shown that the carbonyl compounds investigated in this study have high saturation
110 concentrations (C*, which is inversely proportional to the wall partitioning) and are not affected by line loss (Deming
111 et al., 2019; Li et al., 2023), but line effects such as a broadening of initially sharp concentration peaks cannot be
112 excluded. It has to be noted that sharp concentration peaks or spikes of short duration (< 90 s) were not expected high
113 above the homogenous vegetation of the rainforest. Some less volatile molecules, like sesquiterpenes, never reached
114 saturation and were additionally potentially degraded by O_3 or NO_3 (which was shown to form inside the insulated
115 tubing (Li et al., 2023)); thus, they were not detected. A potential contribution from the oxidation of sesquiterpenes
116 inside the tubing to detected carbonyl species cannot be excluded; however, this contribution is expected to be minor
117 given the rapidly decreasing sesquiterpene concentrations with increasing distance from the canopy (Yee et al., 2018).
118 The residence time in the tubing is short compared to the time that sesquiterpenes are exposed to oxidation during
119 atmospheric transport before reaching the sampling heights. VOC were measured by a Proton Transfer Reaction Time
120 of Flight Mass Spectrometer (PTR-ToF-MS 4000, Ionicon Analytik, Innsbruck, Austria) (Jordan et al., 2009) with a
121 time resolution of 20 seconds and averaged to 4 minutes.

122 Meteorological data were measured at the walk-up tower at multiple heights up to 80 m (LI7500A, LI-COR
123 Biotechnology, Lincoln, USA) and at the tall tower at 325 m (Lufft, WS600-LMB, G. Lufft Mess- und Regeltechnik
124 GmbH, Fellbach, Germany) with a time resolution of 1 minute.

125

2.2   NO+ chemical ionization

127 PTR-ToF-MS in general is a form of chemical ion mass spectrometry (CIMS) commonly operated with hydronium
128 ions (H_3O^+) for the chemical ionization of VOC in air samples. The technique is well-established and sensitive and is
129 able to detect most of the prominent VOC in ambient air with a high temporal resolution of seconds (de Gouw and
130 Warneke, 2007). The proton transfer reaction that lends its name to the instrument occurs between H_3O^+ ions and the
131 molecules R with a higher proton affinity than water (> 691 kJ mol^{-1}) (Hunter and Lias, 1998).

132 $$R + H_3O^+ \longrightarrow RH^+ + H_2O \qquad (R1)$$

133 Thus, isomeric molecules (such as acetone and propanal) form the same product ion RH^+ and cannot be distinguished.
134 For the purpose of investigating the atmospheric chemistry of carbonyl compounds, this is a major disadvantage since
135 the distribution between short-lived aldehydes and longer-lived ketones with the same carbon number remains unclear.
136 However, it has been shown that by using an alternative reagent ion (i.e., NO^+), aldehydes and ketones can be

137   distinguished. NO^+ ionizes aldehydes mainly via hydride abstraction (R2), whereas ketones and NO^+ tend to form a
138   cluster (R3) leading to different product ions (Koss et al., 2016; Španěl et al., 1997).

139                $R + NO^+ \longrightarrow (R\text{-}H)^+ + HNO$ (R2)

140                $R + NO^+ \longrightarrow (RNO)^+$ (R3)

141   To implement the NO^+ chemical ionization mass spectrometer (NO^+ CIMS), synthetic air instead of water vapor was
142   introduced in the ion source, and the source parameters were tuned to achieve a low contribution of impurity ions
143   (H_3O^+, O_2^+, NO_2^+) and high counts of NO^+. Two settings with varying E/N (electrical field strength to gas number
144   density) values were applied. One set had a relatively low E/N of 70 Td (Air (NO) = 9 sccm, U_{drift} = 500 V, p_{drift} =
145   3.4 mbar, T_{drift} = 60 deg C, U_{source} = 70 V), which has been recommended in previous studies to minimize
146   fragmentation (Koss et al., 2016; Romano and Hanna, 2018); the other was operated with 120 Td (Air (NO) = 9 sccm,
147   U_{drift} = 850 V, p_{drift} = 3.4 mbar, T_{drift} = 60 deg C, U_{source} = 70 V) for comparison. Low impurities of H_3O^+ ($\leq$ 1 %), O_2^+
148   (< 0.01 %) and NO_2^+ (< 2.5 %) were achieved using both settings.

149   The identity of the reaction that occurs to ionize the target compound depends on the thermodynamical properties of
150   the molecule. The hydride ion affinity of aldehydes is less than that of NO^+, so R2 is exothermic and favored (Karl et
151   al., 2012; Španěl et al., 1997). Ketones do not show the same tendency to donate a hydrogen atom and the ionization
152   energies of most ketones, especially small ones, is slightly higher than that of NO (> 9.26 eV) (Smith et al., 2003).
153   Thus, an association reaction, R3, primarily occurs for the ketones in this study. Due to the humid conditions in the
154   rainforest, $NO^+(H_2O)$-clusters were also available to react with ketones via ligand switching, producing the same
155   products as the association reaction R3 (Smith et al., 2003). The ionization energies of 3-hexanone, 2-heptanone, and
156   2-nonanone are smaller than or equal to that of NO; nevertheless, the association reaction has been shown to be favored
157   by selected ion flow tube (SIFT) studies (Španěl et al., 1997). Those compounds were, however, not detected in the
158   mass spectra obtained in the rainforest environment examined in this study.

159   Besides the most favored reaction, other ionization channels can also produce product ions. This, and partial
160   fragmentation in the drift tube can lead to additional complications of the mass spectra. To identify the distribution of
161   product ions and fragments of carbonyls for the type of instrument used in this study, a single-compound headspace
162   analysis was performed in the laboratory under humid conditions using a PTR-ToF-MS 8000. This is important as the
163   sensitivity of the carbonyl signals towards water originates from the formation of H_3O^+ ions (and ionized water
164   clusters) that compete with NO^+ and from the formation of NO^+ water clusters. It should be noted that we accounted
165   for the humidity-dependent formation of $(H_2O)NO^+$ by normalizing the signals to NO^+ and $(H_2O)NO^+$. The basic
166   components of the PTR-ToF-MS 8000, mainly the ion source, drift tube, and detector are similar to a PTR-ToF-MS
167   4000, so that the relative transmission can be assumed to be identical. The instrument was tuned to have the same E/N
168   (electric field intensity divided by gas number density) in the drift tube and similar impurities ($\leq$ 5 %) as the instrument
169   in the field. In both field and laboratory, both settings for the E/N values were applied. The results of the single-
170   compound headspace analysis can be found in the Supplementary (Table S1).

171   The complexity of the mass spectra measured with a NO^+ CIMS is a disadvantage if one aims for a non-targeted
172   analysis of VOC present in a certain environment, such as the rainforest. Long-term VOC observations at ATTO are
173   therefore conducted with a PTR-ToF-MS using H_3O^+ ions. However, for a targeted analysis, specifically for separating
174   carbonyl compounds, the NO^+ CIMS is a convenient method (Ernle et al., 2023; Karl et al., 2012; Koss et al., 2016).
175   Another advantage of the NO^+ chemistry is the ability to detect certain alkanes, as their proton affinity is too low to
176   be detected by a PTR-MS (Koss et al., 2016). This has been widely used in urban or rural areas to quantify vehicle
177   emissions, but such species have not yet been investigated at the ATTO rainforest site (Chen et al., 2022; Wang et al.,
178   2020a).

179

2.3   VOC data analysis

Integration of the mass spectra, baseline-, and duty-cycle-correction were performed using the IDA software (Ionicon Analytik). In a subsequent step, the obtained signals were normalized to NO^+ and $(H_2O)NO^+$ and drift parameters like pressure and temperature, to account for fluctuations.

Table 1 shows the sensitivities and limits of detection (LoD) for all target molecules with E/N values of 70 and 120 Td applied. It was evident that the sensitivity of ketones decreases dramatically with high E/N conditions, most probably due to enhanced fragmentation caused by more collisions in the drift tube.

Compounds displayed in bold in Table 1 were quantified using a primary VOC gas standard (Apel-Riemer Environmental Inc., Colorado, USA). The calibration was performed using moisturized synthetic air mixed with the VOC gas standard to mimic tropical conditions with 70 to 95 % relative humidity, typical for the ATTO site. Unfortunately, this did not comprise all target carbonyls, and for those compounds not in the standard, a theoretical method was applied to obtain concentrations, resulting in a higher uncertainty. The relative distribution of the product ions obtained from the single-compound headspace analysis was used to correct for the fragmentation of carbonyl compounds with higher m/z-ratios onto the parent m/z-ratios of other target compounds.

For those compounds not included in the gas standard, mixing ratios were obtained by calculating the ionization efficiency with a previously determined reaction rate of NO^+ and the target compound under the current conditions in the drift tube (k-rate analysis) (Cappellin et al., 2012).

$$[VOC] = \frac{1}{c\,k\,t} \frac{[VOC^+]_{ncps}}{[NO^+]_{ncps}} \tag{1}$$

Here, k is the reaction rate, and t represents the reaction time in the drift tube, which can be approximated using the length of the drift tube, the mobility of the primary ions and the applied drift voltage. Using Equation 1, the mixing ratio of a VOC is calculated from the normalized measured signal (ncps = normalized counts per second) of the main product ion. However, the reaction rates (k-rates), also presented in Table 1, have been experimentally derived for the sum of all product ions. Thus, a weighting factor c for the relative production of the target ion needs to be applied, which was also obtained by the single-compound headspace analysis from the slope of the signals of the target ion vs. other product ions. The mixing ratios of both E/N settings, obtained by applying Equation 1 with the respective product ion distributions, agree well for most compounds (except for n-hexanal and ketones, which have a low sensitivity at 120 Td). This accordance supports the assumption that product ion distributions were valid for both instruments. To calculate propanal, the calibration factor of methacrolein was used, since in a previous calibration measurement with the PTR-ToF-MS 8000 both compounds had similar sensitivities (methacrolein: 0.13 ppb ncps^{-1}, propanal: 0.17 ppb ncps^{-1}).

The measurement uncertainty in the mixing ratios of standard calibrated VOC was less than 25%. It was derived from the accuracy of the VOC gas standard ($\pm$ 5%), the flow meter used for the calibration ($\pm$ 1%), the accuracy of the least square fit of the calibration curve (molecule-dependent, circa $\pm$ 10%), and the uncertainty of the relative distribution of product ions, which was expected to be below 20%. The uncertainty of the product ion distribution was estimated from the purity of the liquid carbonyls tested (> 95%) as well as possible contamination during the headspace sampling. In the case of theoretically calculated mixing ratios using k-rates the accuracy was accordingly higher. The accuracy of the k-rate ($\pm$ 20%) (Španěl et al., 1997) and the accuracy of the distribution of product ions give the absolute accuracy for k-rate calibrated mixing ratios which was thus estimated to be below 30%.

Detection limits were defined as three times the standard deviation of the background noise at the specified mass. Those are also displayed in Figures 1–2. Negative values arising from the subtraction of the background were set to zero to account for a slightly too high background measurement of some compounds during calibration.

2.4   Validation of observations

Pre-separation of the VOC with a GC column prior to detection with the NO$^+$ CIMS can indicate the pureness or compound specificity of an m/z ratio. Koss et al., 2016 reported such data for urban ambient air and concluded that certain masses can be seen as unambiguous in that environment. The E/N field used in that study, which strongly impacts the fragmentation patterns on different m/z ratios, was similar to this study (60 Td), but the measurement site was a parking lot in an urban area (Koss et al., 2016). Uncontaminated m/z ratios assigned to carbonyl compounds were found for acetaldehyde, propanal, methacrolein, and crotonaldehyde, the sum of C$_5$-aldehydes, acetone, hexanal, MVK, methyl ethyl ketone (MEK), benzaldehyde, heptanal, the sum of C$_5$-ketones, and octanal. Nevertheless, biogenic compounds that may not be present in an urban environment were, therefore, not part of the GC method applied in Koss et al. and remained as potential interferents for the carbonyl m/z ratios.

Allyl ethyl ether, an isomer of C$_5$-carbonyls that also undergoes hydride transfer, was potentially such a candidate for interfering in the C$_5$-aldehyde m/z ratio (Smith et al., 2011; Španěl and Smith, 1998). The m/z ratio of C$_5$-aldehydes might have also been affected by 1-5 pentanediol if present at significant concentrations (Španěl et al., 2002). Some carboxylic acids react with NO$^+$ under the drift tube conditions to form R $-$ OH $+$ HNO$_2$ and thus make isomers to the ionized carbonyl species. Trimethylacetic acid was reported to mainly form C$_5$H$_9$O$^+$ and thus can also potentially interfere with C$_5$-aldehydes (Španěl and Smith, 1998).

N-butyric acid is part of the glucose metabolism in plants and, upon ionization, partly makes C$_4$H$_7$O$^+$ ions (m/z 71.0491); thus, it potentially interfered with butanal (Smith et al., 2011). The same holds for isobutyric acid. Also, valeric acid has been shown to fragment into C$_4$H$_7$O$^+$ to a great extent (Ŝpaněl and Smith, 1998). For the alcohols 2-butanol, 1,4-butanediol, and the ester methyl butyrate, fragmentation into C$_4$H$_7$O$^+$ has been shown to occur (Koss et al., 2016; Španěl et al., 2002; Ŝpaněl and Smith, 1998). Tetrahydrofuran, an ether isomeric with butanal is ionized via hydride transfer and also forms C$_4$H$_7$O$^+$ (Španěl and Smith, 1998). Contamination from 2-butanol was shown to account for around 50% of C$_4$H$_7$O$^+$ at an urban site in Boulder, USA (Koss et al., 2016). Since 2-butanol has been previously found in emissions from vegetation (Kesselmeier and Staudt, 1999) and the mixing ratios of C$_4$H$_7$O$^+$ were close to the detection limit, butanal could not be investigated without potential bias from other oxygenated VOC. With another measurement technique (sampling to adsorbent tubes and measurement with a GC-ToF-MS) applied at ATTO also no significant butanal peak was found. However, butanal has been identified in the Amazonian atmosphere during the dry and wet seasons at another site in 1999 (Andreae et al., 2002).

Table 1: List of identified carbonyl compounds and other hydrocarbons and their properties for detection with NO$^+$ CIMS (PTR-ToF-MS 4000). Sensitivities are compared to the classical PTR-MS method using H$_3$O$^+$ reagent ions. *c* represents the weighting factor for the k-rate obtained from the distribution of product ions as described in section 2.3. Compounds in bold were quantified using a primary standard.

				NO$^+$						H$_3$O$^+$
				E/N = 70 Td			E/N = 120 Td			E/N = 120 Td
Carbonyl species	Ion formula	Exact m/z	k-rate 10^{-9} cm^3 s^{-1}	c	Sensitivity ppb ncps^{-1}	LoD ppb	c	Sensitivity ppb ncps^{-1}	LoD ppb	Sensitivity ppb ncps^{-1}
Acetaldehyde	C$_2$H$_3$O$^+$	43.01784	0.6 (Španěl et al., 1997)	-	0.155	0.112	-	0.431	0.160	0.025
Acetone	C$_3$H$_6$NO$_2^+$	88.0393	1.2 (Španěl et al., 1997)	(0.43)	0.078	0.06	0.27	4.803	0.705	0.031
Propanal	C$_3$H$_5$O$^+$	57.0335	2.5 (Španěl et al., 1997)	(0.79)	*0.046*	0.053	0.82	*0.256*	0.049	-
MEK	C$_4$H$_8$NO$_2^+$	102.055	2.8 (Španěl et al., 1997)	(0.84)	0.049	0.008	0.61	1.027	0.111	0.028
MVK	C$_4$H$_6$NO$_2^+$	100.039	2.4 (Michel et al., 2005)	0.86	-	0.004	0.67	-	0.012	-
MACR	C$_4$H$_5$O$^+$	69.03349	2.6 (Michel et al., 2005)	(0.54)	0.046	0.021	0.42	0.256	0.093	0.028
n-pentanone	C$_5$H$_{10}$NO$_2^+$	116.0706	3.4 (Španěl et al., 1997)	0.85	-	0.005	0.56	-	0.007	-
n-pentanal	C$_5$H$_9$O$^+$	85.0648	3.2 (Španěl et al., 1997)	0.79	-	0.003	0.28	-	0.011	
n-hexanone	C$_6$H$_{12}$NO$_2^+$	130.0863	3.3 (Španěl et al., 1997)	-	-	0.002	-	-	-	-
Hexanal	C$_6$H$_{11}$O$^+$	99.0804	2.5 (Španěl et al., 1997)	0.75	-	0.006	0.4	-	0.016	-
Trans-2-hexenal	C$_6$H$_9$O$^+$	97.0672	2.8 (Roberts et al., 2022)	0.68	-	0.006	0.82	-	0.005	-
Benzaldehyde	C$_7$H$_5$O$^+$	105.033	2.8 (Španěl et al., 1997)	0.96	-	0.005	0.97	-	0.003	-
Heptanal	C$_7$H$_{13}$O$^+$	113.0961	2	-	-	0.004	-	-	0.007	-
Octanal	C$_8$H$_{15}$O$^+$	127.1117	2.7 (Romano and Hanna, 2018)	0.81	-	0.004	0.61	-	0.004	-
Nonanal	C$_9$H$_{17}$O$^+$	141.1274	1.1 (Roberts et al., 2022)	0.04	-	0.145	0.1	-	0.078	-
Nopinone	C$_9$H$_{14}$O$^+$	138.1039	2	-	-	0.019	-	-	0.002	-
Alkanes										
Isopentane	C$_5$H$_{11}^+$	71.086	2	-	-	0.013	-	-	0.027	-
Methyl-cyclopentane	C$_6$H$_{11}^+$	83.086	2	-	-	0.005	-	-	0.008	-
2-, 3-methyl-pentane	C$_6$H$_{13}^+$	85.101	2	-	-	0.007	-	-	0.006	-
C$_7$ cyclic alkanes	C$_7$H$_{13}^+$	97.101	2	-	-	0.004	-	-	0.003	-

| | Ion formula | Exact m/z | k-rate 10^{-9} cm^3 s^{-1} | NO$^+$ E/N = 70 Td | | | NO$^+$ E/N = 120 Td | | | H$_3$O$^+$ E/N = 120 Td |
				c	Sensitivity ppb ncps^{-1}	LoD ppb	c	Sensitivity ppb ncps^{-1}	LoD ppb	Sensitivity ppb ncps^{-1}
C2-alkyl-cyclohexanes	$C_8H_{15}^+$	111.117	2	-	-	0.004	-	-	0.005	-
Alkenes										
C$_5$-alkene (2-pentenes)	$C_5H_{10}^+$	70.0777	2	-	-	-	-	-	0.009	-
C$_5$-alkene (a-olefin)	$C_5H_{10}NO^+$	100.076	2	-	-	0.006	-	-	0.003	-
C_6H_{10}	$C_6H_{10}^+$	82.0777	2	-	-	0.006	-	-	0.01	-
Alcohols										
Ethanol	$C_2H_5O^+$	45.0335	2	-	-	0.050	-	-	0.019	-
Alkyne										
Propyne	$C_4H_6^+$	54.046	2	-	-	0.026	-	-	0.011	-
Aromatic										
Benzene	$C_6H_6^+$	78.046	-	-	0.101	0.020	-	0.071	0.009	0.063
Terpenes										
Isoprene	$C_5H_8^+$	68.0621	-	-	0.078	0.018	-	0.068	0.023	0.045
Sum of mono-terpenes	$C_{10}H_{16}^+$	136.125	-	-	0.067	0.004	-	0.554	0.039	0.103
Other										
Furan	$C_4H_4O^+$	68.0258	2	-	-	0.008	-	-	-	-
$C_5H_4O_3$	$C_5H_4NO_4^+$	142.014	2	-	-	0.005	-	-	0.003	-

251 Propionic acid is a potential contaminant for propanal on the m/z of $C_3H_5O^+$, but only a fraction of the acid was found
252 to land on the propanal m/z (Ŝpaněl and Smith, 1998). A higher fraction of the fragments of methyl and ethyl
253 propionate were detected as isomers to ionized propanal but have not been found to be present in biogenic emissions
254 so far (Kesselmeier and Staudt, 1999; Ŝpaněl and Smith, 1998).

255 It can also not be excluded that fragmentation to $C_2H_3O^+$ of several species, in particular acetic acid, methyl formate,
256 methyl acetate, and ethyl acetate contributes to the m/z ratio of acetaldehyde ($C_2H_3O^+$). Experimental evidence for the
257 contamination has only been found for a small contribution of methyl and ethyl acetate of less than 20% (Ŝpaněl and
258 Smith, 1998).

259 The isomers hexanal and z-3-hexenol are known to be emitted together by damaged green leaves (Jardine et al., 2012a;
260 Langford et al., 2010). A possible detection of both compounds on m/z of $C_6H_{11}O^+$ could not be excluded, since
261 alcohols also undergo hydride abstraction during the reaction with NO$^+$ (Koss et al., 2016).

262 To our knowledge, none of the species that were demonstrated to fragment on the same m/z ratios as carbonyls have
263 been reported to be abundant in forested environments or even to be biogenically emitted, except for z-3-hexenol, 2-
264 butanol, n- and isobutyric acid, acetic acid, and propionic acid. In general, acids have primary sources, including
265 biogenic emissions and biomass burning but also photochemical sources including the ozonolysis of alkenes
266 (Orzechowska et al., 2005). The dataset from this study and comparison with the corresponding m/z of acids under

267 H_3O^+ ionization that have been measured previously at the ATTO site suggested that carboxylic acids undergo an
268 association reaction with NO^+. A headspace analysis with acetic acid also revealed no significant contributions to any
269 other m/z except the association product $C_2H_4NO_3^+$.

270 Fragmentation from higher carbonyls to m/z ratios attributed to lower carbonyls was observed in the single compound
271 headspace analysis, conducted with aldehydes and ketones up to nonanal. The m/z of acetaldehyde ($C_2H_3O^+$, 43.0178)
272 saw small contributions from acetone and pentanone, which were subtracted from the acetaldehyde signal. For this
273 correction, the relative contribution of the fragments from their parent mass, which was determined by the headspace
274 analysis, was used. A list of the single compounds and their product ions formed in the drift tube can be found in the
275 supplementary Table S1. Contributions from higher carbonyls in the NO^+ CIMS were not likely since they were not
276 observed or were below the detection limit.

277

3   Results

3.1   Atmospheric conditions and seasonality

280 Seasonality in the central Amazon is characterized by a comparatively less polluted wet season (February–May) and
281 a more strongly polluted dry season, due to the more frequent influence of biomass burning (August–November)
282 (Holanda et al., 2023; Pöhlker et al., 2019). The NO^+ CIMS measurements took place from June 23 until July 8 and
283 from September 27 until October 14, 2019. Below, we outline the meteorological conditions during both measurement
284 periods as they influenced seasonal variations in observed VOC mixing ratios and correlations. It is important to
285 consider that the photochemical loss of VOC and reactions involving OH depend on the availability of sunlight, which
286 also affects the secondary formation of OVOC from the oxidation of different hydrocarbons. VOC emissions from
287 vegetation are driven by light (photosynthetically active radiation, PAR), temperature, water availability, air pollution,
288 and biotic factors, such as herbivore infestation, pathogenic infections, or the developmental stage of a plant
289 (Laothawornkitkul et al., 2009). However, at heights above 80 m, integrated VOC emissions from a whole forested
290 area domiciled by various plant and herbivorous species at all developmental stages were sampled. As has been
291 reported previously, inter-seasonal growth variations may even induce the plant to switch from isoprene emission to
292 monoterpene emission and back (Kuhn et al., 2004a, b). The growth of new leaves (leaf flush), which are
293 photosynthetically more effective than mature leaves peaks in the dry season and is correlated with the availability of
294 light (Restrepo-Coupe et al., 2013), which causes an inter-seasonal gradient possibly manifested in the presented
295 BVOC emissions. The emission and uptake of BVOC by soils and cryptogamic organisms was shown to depend on
296 the availability of water and could additionally contribute to observed seasonal differences in BVOC concentrations
297 (Bourtsoukidis et al., 2018; Edtbauer et al., 2021).

298 On average, daytime temperatures differed by only 0.4 °C between the transition (June – July) and the dry season
299 (Fig. S3). Maximum temperatures in the canopy (at 26 m) were reached at 12:00 local time (LT), with 30.5 °C in the
300 transition season and 31.2 °C in the dry season on average. The diurnal evolution of temperature closely followed the
301 incoming solar radiation, here represented by PAR. Dry season observations of PAR were higher by about 9%
302 compared to the transition season. Precipitation in the month before the NO^+ CIMS measurements took place totaled
303 157 mm in June and 119 in September 2019 (Fig. S4). The water level measured in the Rio Negro close to Manaus in
304 2019, however, exhibited maximum values in June and minimum values in October, with a difference of about 10 m
305 (Chevuturi et al., 2022).

306 The sampled air originated predominantly from the east (SE to NE); thus, an influence from the city of Manaus could
307 be excluded (Fig. S1). However, for long-lived anthropogenic alkanes, influence from populated areas along the
308 Amazonas and smaller side rivers was conceivable. The detected alkanes (Table 1) had low mixing ratios below the
309 detection limit, indicating no significant influence from industries based on fossil fuel combustion.

310 Black carbon (BC) was used as a marker of biomass burning emissions. BC sampled at ATTO has been shown to
311 originate from biomass burning in South America and Africa (Holanda et al., 2020, 2023). Enhanced concentrations
312 of 0.42 and 0.54 µg m^{-3} (80, 325 m) were found on average in the 2019 dry season. Maximum concentrations reached

313 0.93 and 1.17 µg m^{-3}. Average concentrations of 0.18 and 0.21 BC (80, 325 m) in the transition season indicated less
314 polluted conditions. A large number of VOC, including certain carbonyl compounds, are usually co-emitted during
315 biomass burning with various emission factors and rates (Andreae, 2019; Andreae and Merlet, 2001). Therefore, the
316 carbonyls detected with the NO$^+$ CIMS during this study and their precursors potentially originated from both biogenic
317 and biomass burning sources. Correlations of carbonyls with BC at 325 m are shown in the Supplementary Data for
318 both seasons (Fig. S5) to detect possible influences from advected, fresh, or aged biomass burning plumes. In the cases
319 of acetaldehyde, acetone, methacrolein, MVK, and benzaldehyde, a Pearson coefficient of $p > 0.55$ was calculated for
320 the day and nighttime so that an influence of biomass burning through co-advection or in plume production was
321 feasible.

322

3.2   Vertical distribution of carbonyls above the canopy

324 The distribution of carbonyls with height above the uniform rainforest-covered landscape provides information on the
325 nature of emission sources, oxidative transformations, and carbonyl sinks under consideration of dynamic processes
326 in the atmospheric mixed layer. Vertical gradients were governed by the strength and temporal variance of the
327 respective source and of surface uptake, the atmospheric lifetime of the species considered, and dilution through
328 turbulent mixing or entrainment from the free troposphere during mixed layer growth. Earlier work investigated the
329 chemical and dilutive loss of isoprene with height using observations at ATTO and a turbulence-resolving large eddy
330 simulation (DALES). It was shown that slightly more than 50% of the isoprene loss in the vertical (80–325 m) at noon
331 occurred due to dilutive turbulent mixing (Ringsdorf et al., 2023). It is important to note that the lowest sampling
332 height at 80 m was within the roughness sublayer. This is a layer within the mixed ABL of about 2–3 times the canopy
333 height (≈ 35 m), which is strongly affected by the tall canopy with respect to wind fields and, thus, turbulence. Within
334 this layer, the exchange between the canopy and atmosphere occurs by inhomogeneous flows into and out of the
335 canopy (Chamecki et al., 2020). An important process influencing the ambient concentration of the compounds
336 presented at all sampling heights was the growth of the ABL (up to 2 km height) after sunrise due to the strengthening
337 of turbulences from thermal expansion of the heated air masses near the ground. During ABL growth, air from higher
338 altitudes (residual
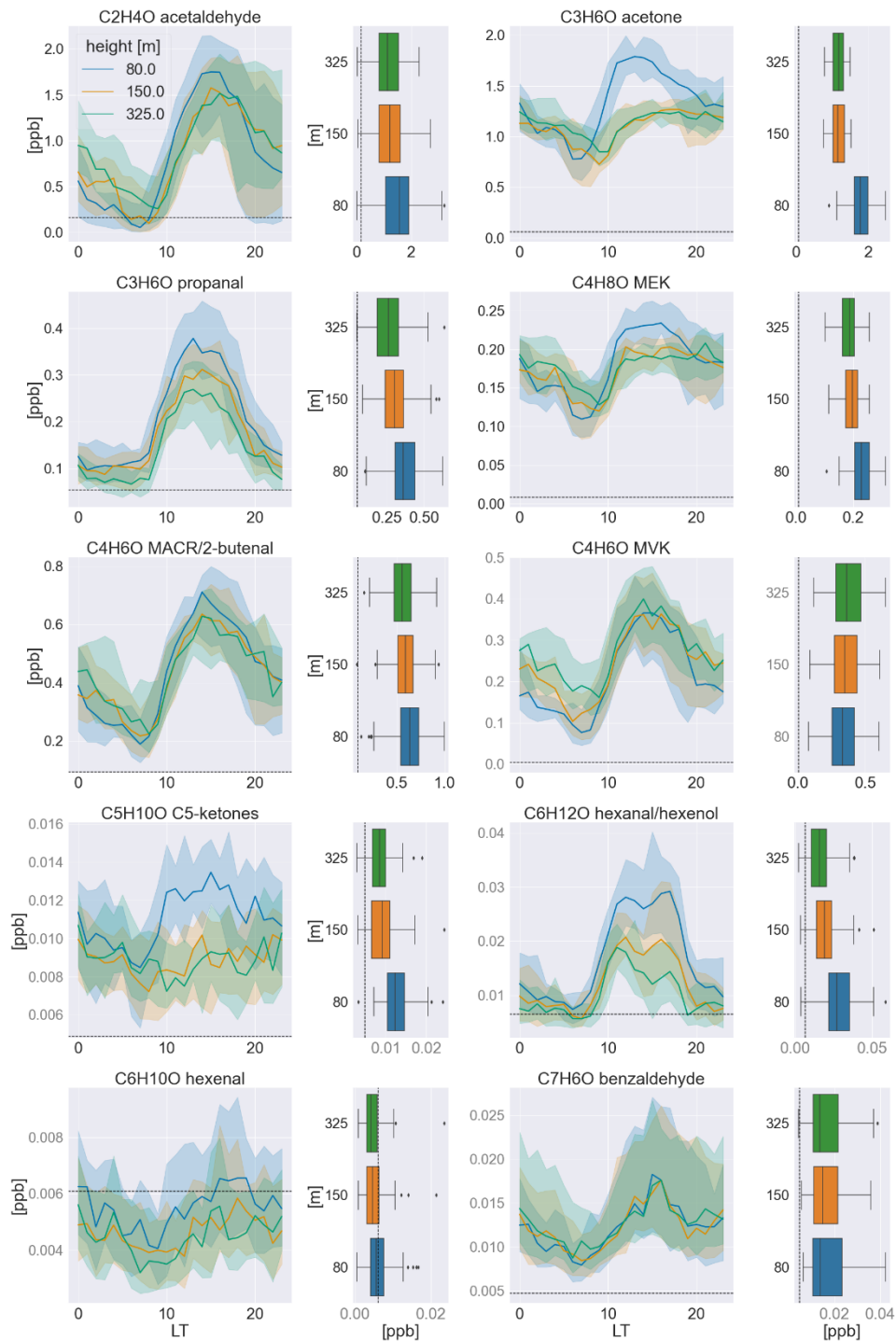
339

Figure 1: Median averaged timeseries in the wet–to–dry transition season (June/July) of 2019 measured at all sampling heights for each carbonyl compound and its respective vertical profile at noon (12:00–15:00 LT) to the right. The shadings indicate the quartiles (25th and 75th). In the box-and-whisker plots, the boxes also represent the quartiles, while the residual data except for outliers are included in the whiskers. The detection limit (3 sigma) is indicated by dashed, black lines. The mixing ratios in black font were calibrated to a standard, while those in gray font were calculated based on the k-rate.

340

341 layer containing more chemically aged air) is entrained, leading to the minimum mixing ratios observed after 06:00 LT
342 at all three heights. During the day, turbulent mixing via convection and associated downward motions is strongest
343 until convection eases with decreasing insolation. At night, a stable stratification associated with low vertical mixing
344 is formed (Jordi Vilà-Guerau de Arellano, et al., 2015).

345 Under the reasonable assumption of a carbonyl source at canopy level (based on emission inventories discussed in
346 section 4), the long-lived ketones were expected to have a background concentration in the convective mixing layer
347 but also above, while levels of short-lived aldehydes will tend to be zero at higher altitudes, analogous to isoprene.
348 Consequently, the aldehydes should show a stronger decrease in their vertical profiles than the ketones, which were
349 expected to be well-mixed at about a hundred meters above the canopy throughout the convective mixing layer.
350 Nonetheless, one has to also take the secondary chemical formation of carbonyls into account, which can influence
351 the vertical gradients depending on the emission source and atmospheric lifetime of the precursors.

352 Figures 1 and 2 present the diurnal cycle observed at the three sampling heights for all carbonyls measured in the wet–
353 to–dry transition and the dry season, respectively. Some compounds were measured in very low concentrations, below
354 the detection limit in one or both seasons, namely, the sum of C_5-aldehydes, C_6-ketones, heptanal, octanal, and
355 nonanal. All other carbonyls showed distinct diurnal variabilities with increasing concentrations after sunrise
356 (06:00 LT) and decreasing concentrations at nighttime. Their diurnal cycle followed the evolution of PAR and
357 temperature with a slight delay throughout the day, reflecting the expected biogenic emission and photochemical
358 production. Time series of the aldehydes and ketones are provided in the supplementary (Fig. S6-S15). As
359 hypothesized above, no significant vertical variability was found for ketones, though only at 150 and 325 m, whereas
360 a strong decrease in mixing ratio with height was observed between 80 and 150 m. This distribution indicates that
361 mixing ratios of ketones were only well-mixed above 150 m, while the measurements at 80 m were influenced by a
362 strong source of ketones, which is discussed compound-wise below. The observed aldehydes exhibited different
363 vertical distributions; some showed increasing mixing ratios with height, others were rather steadily decreasing as it
364 was hypothesized, and some showed very small variabilities throughout the lowermost 325 m of the atmosphere.

365

3.3   Correlations at 80m and common sources

367 The chemical composition of airmasses measured at 80 m was governed by various processes occurring from the leaf
368 level up to mixing scales of the lower atmosphere. At the leaf level, BVOC are formed by plant metabolic pathways
369 or, possibly, in the case of OVOC, including carbonyls via within-leaf reactions. Epicuticular waxes, also called leaf
370 waxes, consist of long-chained hydrocarbons, e.g., the triterpene squalene, which yield OVOC during ozonolysis.
371 Depending on the position of the double bond of the long-chained molecule and its functional groups, aldehydes or
372 ketones are formed, whereby the chances for the formation of short-chained carbonyls like acetone are highest
373 (Fruekilde et al., 1998). Following their emission, a fraction is deposited on surfaces, which is in most cases reversible,
374 or taken up by stomata, which represents a potential sink (Niinemets et al., 2014). Depending on their atmospheric
375 lifetime, BVOC undergo within-canopy oxidation; in the case of reactive isoprene and monoterpenes, this was found
376 to come to not more than 10% of their initial emission flux (Fuentes et al., 2022; Karl et al., 2004) before being ejected
377 from the canopy. Within and above the canopy they are mixed
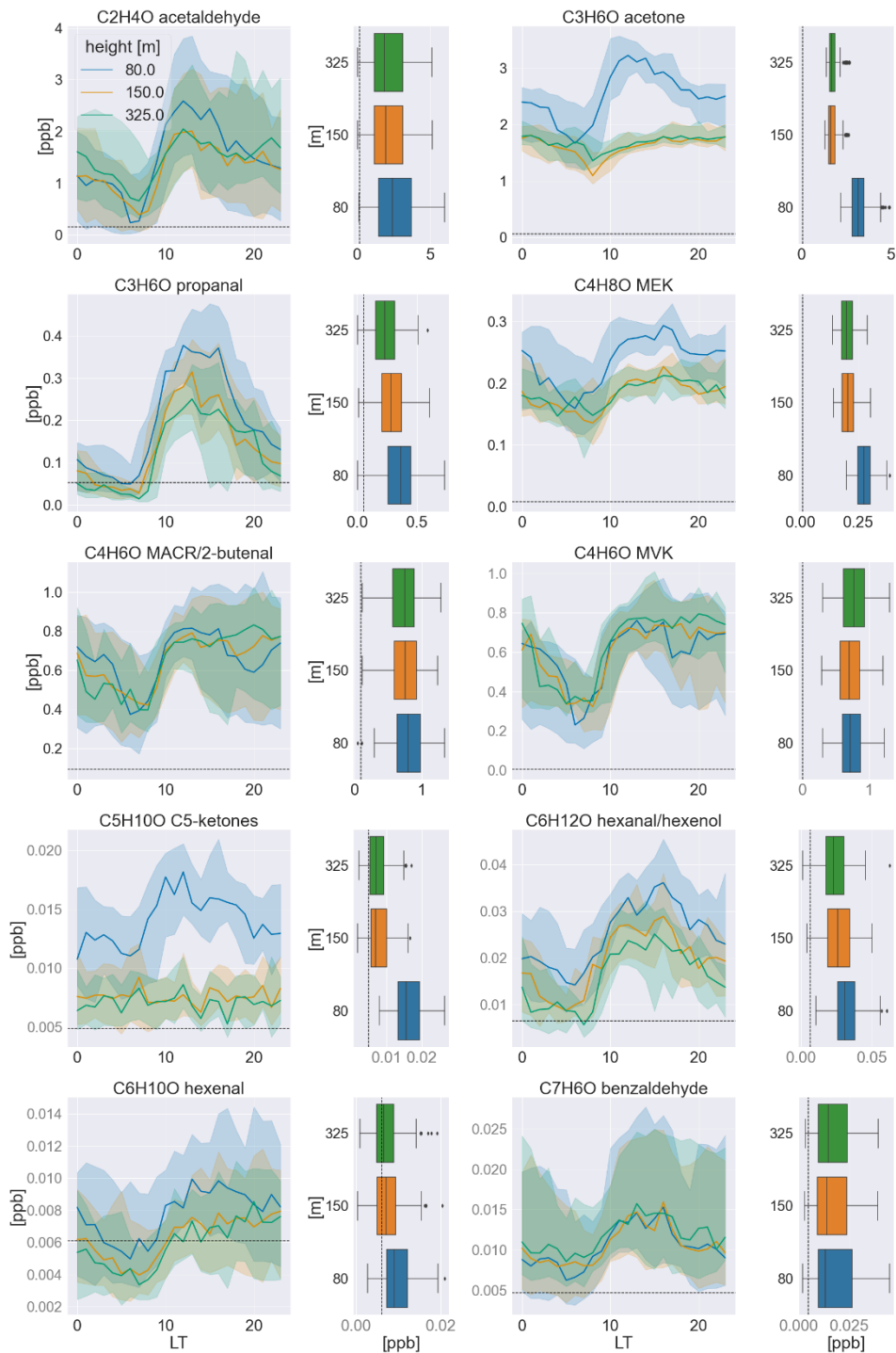
378

379

Figure 2: Median averaged timeseries in the dry season (September/October) of 2019 measured at all sampling heights for each carbonyl compound and its respective vertical profile at noon (12:00–15:00 LT) to the right. The shadings indicate the quartiles (25th and 75th). In the box-and-whisker plots, the boxes also represent the quartiles, while the residual data except for outliers are included in the whiskers. The detection limit (3 sigma) is indicated by dashed, black lines. The mixing ratios in black font were calibrated to a standard, while those in gray font were calculated based on the k-rate.
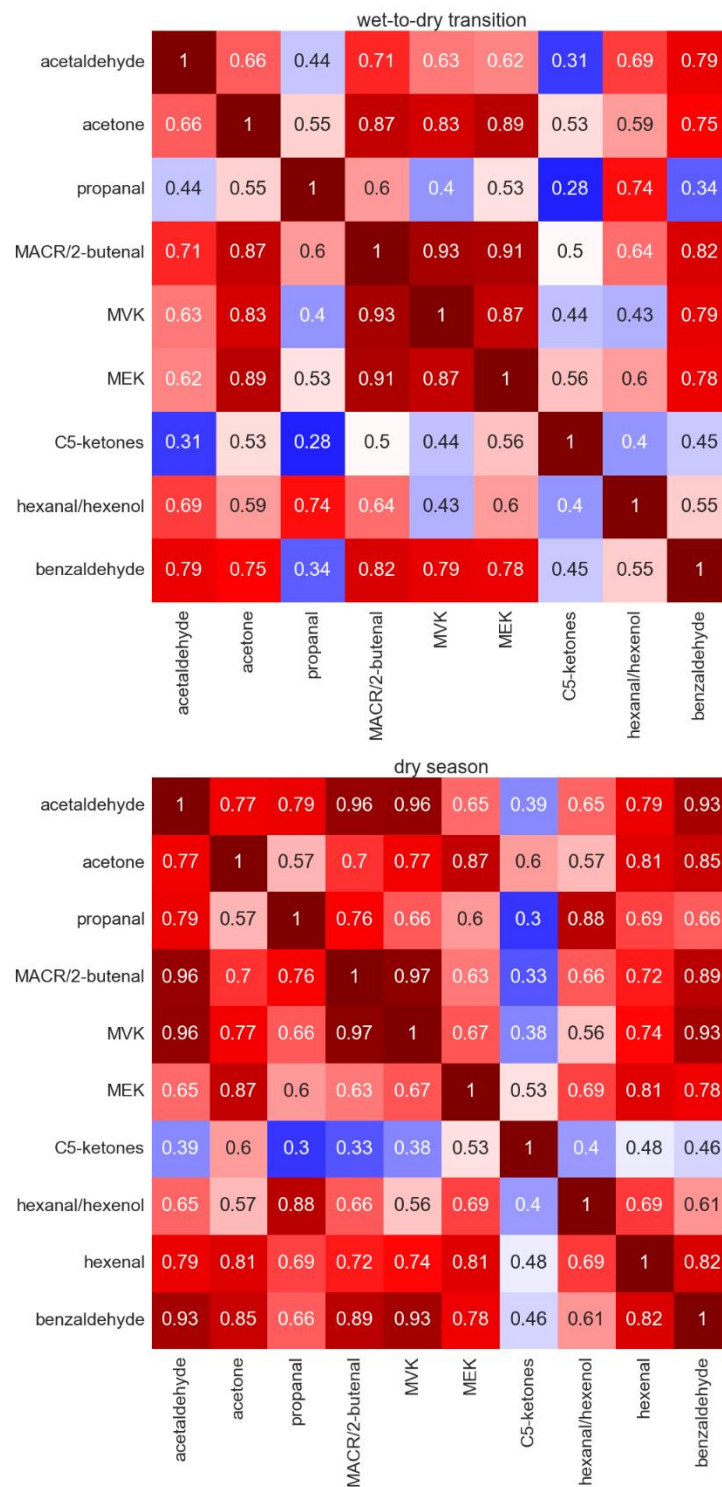
Figure 3: Pearson correlation coefficients for the intercorrelation of carbonyl species in the wet–to–dry transition season (upper) and in the dry season (lower).

air masses of varying ages and secondary production and depletion take place simultaneously. When correlating two time series of BVOC measured at that height, a high correlation coefficient can indicate similar production and loss

383 or possibly a precursor–product relationship. Here, it is very important to consider the timescales of production and
384 loss versus vertical transport since the residence time of airmasses in the first 80 m is limited during daytime
385 convective conditions. In a previous study, the mixing timescale, which accounted for turbulent up and downward
386 motions between 80 and 325 m at ATTO, was determined to range on average from 60 minutes at 10:00 LT to 15 min
387 at 15:00 LT (Ringsdorf et al., 2023). Based on that study, we assumed the mean residence time between the canopy
388 and 80 m to be in the same time range of minutes to 1 hour. Carbonyl precursors including alkenes, isoprene, higher
389 terpenes, and alkanes have atmospheric lifetimes with respect to oxidation by OH radicals of $\tau > 2$ hours, $\tau \approx 3$ hours,
390 minutes to hours, and days to weeks for the much less reactive alkanes (Altshuller, 1991; Wolfe et al., 2011). The
391 lifetimes with respect to OH of carbonyl compounds themselves range from 12 hours (trans-3-hexenal) (Jiménez et
392 al., 2007) to 119 days (acetone) and are even shorter when considering photolysis, which is a significant sink for
393 carbonyls (Mellouki et al., 2015). In Table 2, the lifetimes of carbonyls with respect to an average OH concentration
394 of 1×10^6 molecules cm^{-3} based on a previous study at the ATTO site are presented. This is the average over roughly
395 the same time of day that was considered for carbonyl correlations (10:00–15:00) (Ringsdorf et al., 2023). However,
396 isoprene oxidation was observed by the daily increase of the product MVK between 80 and 325 m.

397 Thus, correlations at 80 m will reflect only the processes that occur on a comparable or faster timescale than mixing.
398 This includes primary emissions, product formation in the atmosphere from short-lived precursors like alkenes and
399 terpenes, and progressive photochemical degradation/photolysis of short-lived carbonyls as well as loss via deposition.

400 Figures 3-4 show the Pearson correlation coefficients (p) for both seasons divided into day (10:00–17:00 LT) and
401 nighttime (22:00–05:00 LT) between the carbonyl compounds and between carbonyls and other selected VOC,
402 including terpenes (isoprene, sum of monoterpenes), alkenes (C_5-alkenes, benzene), and oxygenated compounds
403 (ethanol, furan, acetic acid, $C_5H_4O_3$), when measured above the detection limit. Their diel and vertical distributions
404 are presented in the supplementary figures S16–S17. $C_5H_4O_3$ is a highly oxygenated compound, which was classified
405 to be exclusively an oxidation product of very reactive BVOC in a previous study conducted within and above a pine
406 forest. Therein, emission rates of very reactive BVOC were estimated to reach 6–30 times the emission rates of
407 monoterpenes (Holzinger et al., 2005). In this study, the highest mixing ratios were found at 325 m, suggesting that
408 besides being formed as a first-order oxidation product close to the canopy it was also a higher-order oxidation product
409 that therefore emerges at longer timescales. Very reactive BVOC presumably also represent precursors for carbonyl
410 compounds. Periods with precipitation were excluded from the correlations to avoid the effects of downbursts and
411 washout. As expected, high correlations were found between isoprene and the sum of monoterpenes, which are all
412 primary emissions that depend strongly on light and temperature. Correlation of carbonyl compounds with isoprene
413 and monoterpenes was preferred over PAR and temperature to identify light- and temperature-dependent direct
414 emission, due to the temporal delay between emission and detection. However, it is striking that most carbonyls
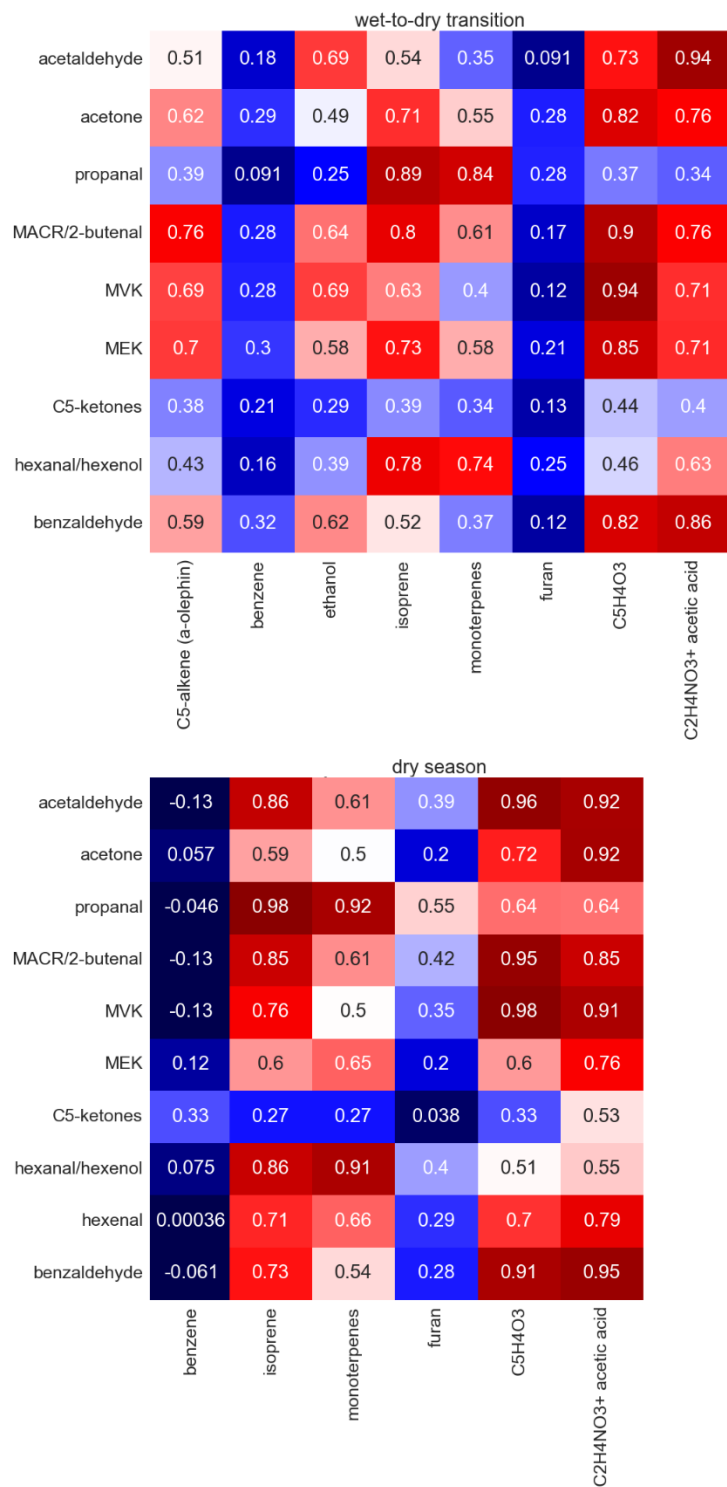
Figure 4: Pearson correlation coefficients for the correlation of carbonyl species with selected hydrocarbons in the wet–to–dry transition season (upper) and the dry season (lower).

415   showed significant correlations with all other carbonyls with Pearson coefficients greater than 0.7. This likely resulted
416   from the common driving variables, namely light and temperature for emission, as well as similar photochemical

417   production rates.

418   The highest correlations with the primary emitted isoprene and monoterpenes were obtained for propanal and n-
419   hexanal. Other compounds that were found to correlate very well were acetaldehyde, methacrolein, MVK, and $C_5H_4O_3$
420   as well as acetone and MEK.

421   **3.4   Nocturnal loss rates**

422   Biogenic emissions unrelated to photosynthesis might have continued during the night, whereas oxidative chemistry
423   and, thus, secondary production of carbonyls was limited to reactions with O_3 and NO_3, which were found at low
424   levels in the remote forested atmosphere. Important loss mechanisms at night are deposition to surfaces and reaction
425   with NO_3 (Brown and Stutz, 2012). Deposition at night is thought to happen via adsorption to the cuticle of the leaves,
426   since stomata are closed in the absence of light. However, there is evidence that the stomatal conductance is maintained
427   at night by many woody species, implying an irreversible uptake for BVOCs that can be further processed and
428   converted to other metabolites (Niinemets et al., 2014). Reaction with NO_3 at nighttime is limited to unsaturated
429   BVOC but is also efficient for some saturated aldehydes. Assuming a rather high mixing ratio of 10 ppt NO_3 (Brown
430   and Stutz, 2012; Khan et al., 2015), nighttime atmospheric lifetimes of 8 days are estimated for n-hexanal, the most
431   reactive observed aldehyde with respect to NO_3. Ozone is circa 1000 times more abundant than NO_3, but the reaction
432   rates with carbonyls are much lower. Therefore, deposition is expected to be the dominant loss mechanism for
433   carbonyls at night. Table 2 summarizes properties of the observed carbonyl compounds that are important driving
434   variables of deposition on surfaces together with their observed loss rates during the night. These rates were obtained
435   by linear regression of the observed nocturnal time series at 80 m between 22:00 and 04:00 LT. Since the uptake of
436   BVOC by leaves occurs only when the ambient concentration exceeds the concentration in the inter-leaf space, high
437   loss rates were observed for BVOC with high ambient mixing ratios. However, the concentration gradient can be
438   maintained by a metabolic transformation of the BVOC in the leaf. Table 2 also includes the reactivity of BVOC
439   towards the OH radical, O_3, and NO_3.

440

441   **4   Discussion**

442   In the following sections, the diel variability, vertical distribution (80–325 m), and correlations between all measured
443   BVOC are considered in a compound-wise manner. The measurements presented here are related to previous studies
444   on the emission, formation, and loss of the carbonyl species.

445   **4.1   Acetaldehyde**

446   Acetaldehyde (ethanal) is known to be an important contributor to the total ambient carbonyl concentration in the
447   atmosphere. Various sources of acetaldehyde have been characterized previously, including direct emissions from
448   vegetation and the ocean and secondary production from the OH-, NO_3-, and O_3-initiated photooxidation of
449   hydrocarbons (Rottenberger et al., 2004; Wang et al., 2020b). Direct biogenic emissions may be of special importance
450   for the Amazonian rainforest, as acetaldehyde and ethanol release have been reported to result from root anoxia
451   (Bracho-Nunez et al., 2012; Holzinger et al., 2000; Rottenberger et al., 2008). This may occur in large areas caused

Table 2: Rate coefficients for the reaction with OH, NO₃, and O₃ and the atmospheric lifetime considering an OH radical concentration of 1×10^6 molecules cm^{-1}. The rate coefficients and boiling point temperature were taken from the NIST database. Water solubility has been reported by Sander et al., 2023. The loss rate is calculated based on the median averaged slopes of the nocturnal (22:00–04:00) carbonyl timeseries.

VOC species	k_{OH} [cm³ #⁻¹ s⁻¹]	Estimated lifetime Amazon [days]	k_{NO3-} [cm³ #⁻¹ s⁻¹]	k_{O3} [cm³ #⁻¹ s⁻¹]	Volatility (T_{boil} [K])	Water-solubility (H_s^{cp}) [mol m⁻³ Pa⁻¹]	Loss rate [ppb min⁻¹] (transition, dry season)
Acetaldehyde	1.6E-11	1.4	2.4E-15	3.4E-20	294	1.3E-1	-6.7E-4, -1E-3
Acetone	1.9E-13	119.3	8.5E-18	8.5E-18	329	2.7E-1	-7.8E-4, -9.5E-4
Propanal	2E-11	1.2	6.2E-15	-	322	9.9E-2	-8.9E-5, -1.4E-4
MEK	1.2E-12	19.3	-	2.06E-16	353	1.8E-1	-8.4E-5, -7.4E-5
MVK	1.9E-11	1.25	1.2E-16	4.48E-18	354	4.0E-1	-1.1E-4, -4.8E-4
MACR	3E-11	0.75	3.3E-15	1.09E-18	341	4.5E-2	-2.1E-4,
2-Butenal	3.6E-11	0.64	5.1E-15	1.58E-18	375.5	5.9E-1	-2.1E-4
2-pentanone (C₅-ketones)	4.6E-12	5.08	-	-	375	1.3E-1	-
n-hexanal	2.8E-11	0.83	1.1E-14	-	402	4.5E-2	-2E-6
Z-3-hexenol	1E-10	0.21	2.7E-13	6.4E-17	427.7	-	-
z-2-hexenal	4.4E-11	0.52	1.2E-14	2.0E-18	419.7	1.4E-1	-
Benzaldehyde	1.3E-11	1.78	2.01E-15	2.0E-19	452	4.0E-1	-7.9E-6, -8E-6
Isoprene	1E-10	0.23	6.7E-13	1.28E-17	307	1.3E-4	-1.5E-3, -2.6E-3
α-pinene	5.3E-11	0.43	6.2E-12	9.6E-17	430	7E-4	1.7E-4, -3.2E-4

by seasonal flooding (Parolin et al., 2004). At 80, 150, and 325 m in the wet–to–dry transition season of 2019, observed mean diurnal concentrations were 642, 702, 852 ppt, respectively, and 1.38, 1.25, 1.47 ppb in the dry season of 2019.

Metabolic production pathways of acetaldehyde within plants and subsequent emission have been found to occur not only during root-flooding but also during rapid light-dark transitions (Fall, 2003; Holzinger et al., 2000). The anaerobic conditions at the root's surface during flooding cause the ethanolic fermentation pathway to form ethanol that is transported to the leaves of the plant to provide an energy source.

Acetaldehyde is an intermediate of this pathway which tends to leak out to the atmosphere due to its high volatility (Kreuzwieser et al., 2000). Some Amazonian tree species can switch to fermentative metabolism (Bracho-Nunez et al., 2012), but concentration or flux measurements during the dry–to–wet transition in Amazonia under field conditions are missing. In this study, a strong correlation was found for ethanol and acetaldehyde in the nighttime during the transition season (p = 0.92). The high correlation coefficient at 80 m could originate from similar sinks, such as deposition to the canopy or related sources, such as the ethanolic fermentation pathway. Ethanol mixing ratios were ten times higher in the transition season and showed a diel maximum at nighttime. Since river levels were at their maximum levels in the transition season, root flooding may be partially responsible for the seasonal variability

Table 3: Median averaged mixing ratios of the observed carbonyl compounds for the measurement periods in the dry–to–wet transition and the 2019 dry season. The range presents the lowest mixing ratio included in the 25th and the highest mixing ratio included in the 75th quantile of the median averaged diurnal cycle. Numbers in italics represent the limit of detection.

Carbonyl species	Height [m]	Wet-to-dry transition – Jun-Jul 2019		Dry season 2019 – Sep-Oct 2019	
		Median [ppt]	Range [ppt]	Median [ppt]	Range [ppt]
Acetaldehyde	80	642	24 - 2043	1380	*160* - 3179
	150	702	24 - 1801	1252	239 - 3134
	325	852	59 - 1883	1472	256 - 3716
Acetone	80	1333	559 - 2083	2546	1155 - 3812
	150	1124	494 - 1509	1657	918 - 2105
	325	1146	661 - 1545	1707	1087 - 2115
Propanal	80	176	71 - 438	165	*53* - 410
	150	150	58 - 365	115	*53* - 349
	325	119	*53* - 348	85	*53* - 305
MEK	80	177	82 - 267	249	116 - 348
	150	175	81 - 229	188	98 - 259
	325	177	105 - 240	185	75 - 247
MVK	80	184	45 - 483	607	100 - 994
	150	229	53 - 481	599	164 - 967
	325	265	93 - 499	659	239 - 1014
MACR/2-Butenal	80	415	149 - 755	679	250 - 1026
	150	425	149 - 697	644	307 - 1010
	325	439	181 - 694	644	281 - 996
C_5-ketones	80	11	*7* - 18	14	*7* - 23
	150	9	*7* - 15	8	*7* - 13
	325	9	*7* - 15	*7*	*7* - 12
n-hexanal/ hexenols	80	15	*6* - 50	26	*6* - 53
	150	11	*6* - 33	19	*6* - 42
	325	9	*6* - 30	16	*6* - 43
z-2-hexenal	80	-	< 11	8	*6* - 14
	150	-	< 9	-	< 12
	325	-	< 9	-	< 12
Benzaldehyde	80	12	*6* - 27	11	*6* - 26
	150	12	*6* - 24	10	*6* - 26
	325	12	*6* - 24	11	*6* - 25

466 of ethanol (Kirstine and Galbally, 2012). However, acetaldehyde showed a different seasonal variability, indicating
467 that other sources than those of ethanol were dominant. It is important to keep in mind that the ATTO site is a "Terra
468 firme" region with inundation events rare. Field measurements of roots under anoxia are still missing. Fast light–dark
469 transitions occur continuously inside the forest canopy and are suspected to lead to an overproduction of cytosolic
470 pyruvic acid in the leaves that is converted to acetaldehyde as a safety mechanism against acidification (Fall, 2003).
471 The wounding of a plant through cutting or drying out of plant tissues also leads to release of acetaldehyde (Guenther,
472 2000). The compound is also found in emissions from leaf litter presumably as a byproduct of biomass degradation
473 (Karl et al., 2003; Schade and Goldstein, 2001). Furthermore, the oxidation of polyunsaturated fatty acids in leaves
474 leads to the formation of reactive aldehydes, which can represent a primary source for many aldehydes, including
475 acetaldehyde (Matsui et al., 2010; Niinemets et al., 2014). Once released, the atmospheric lifetime of acetaldehyde is
476 in the range of 1.4 days with respect to OH (Table 2).

477   Tree branch enclosures and vertical gradient measurements at another Amazonian measurement site (Rondônia) in
478   1999 revealed that the canopy's role as a sink can even exceed its function in emissions. Uptake to leaves mainly
479   occurred via the leaf stomata and has been reported to be governed by a compensation point that varies between
480   canopy and understory species. The authors concluded that the observed ambient concentrations were generated
481   mainly by the secondary photochemical production of acetaldehyde (Rottenberger et al., 2004). Accordingly, in 2013,
482   measurements of acetaldehyde using a PTR-quadrupole-MS (nominal m/z 45) vertical gradients below 80 m at ATTO
483   showed increasing acetaldehyde between 24 m (inside the canopy, high influence by surrounding trees) and 79 m.
484   However, interestingly, this has only been observed in the dry season (Sep), whereas during the wet season of 2013
485   (Feb/Mar), a dominance of primary emission over secondary production was indicated by decreasing concentrations
486   directly above the canopy (Yáñez-Serrano et al., 2015). We observed decreasing mixing ratios at altitudes above 80 m
487   under dry season or close to dry season conditions in 2019. At noon, the acetaldehyde mixing ratios peaked in the first
488   150 m above the canopy, consistent with a rapid secondary production and a possible contribution from direct
489   emission. Primary emission might vary in strength and dominance with season due to the variability of light,
490   temperature, precipitation, and soil moisture and due to plant phenology. At 150 and 325 m, similar mixing ratios
491   were measured, suggesting well-mixed conditions and ongoing secondary formation between those heights, due to the
492   many routes of acetaldehyde photochemical generation.

493   In the rainforest environment, sources of the photochemical precursor hydrocarbons of acetaldehyde are most likely
494   to be natural emissions or longer-lived emissions from distant biomass burning. Aldehydes are a common product of
495   any hydrocarbons that are oxidized in the atmosphere (Calogirou et al., 1999; Mellouki et al., 2015). Laboratory
496   experiments showed that acetaldehyde emerges from the oxidation of alkanes and alkenes, with ethane and propene
497   having the largest emission fluxes globally (Singh et al., 2004). Ethane is globally distributed; thus, background
498   concentrations of acetaldehyde are generated by this route, which are, however, low due to the rapid subsequent
499   transformation via reaction with OH. Biogenically emitted compounds with high molar yields for the formation of
500   acetaldehyde are $> C_2$ alkenes (0.85) and ethanol (0.95). Additionally, isoprene and terpenes have a low molar yield
501   (0.019, 0.025) but exhibit the strongest emissions measured from the forest (Fischer et al., 2014). The reaction of other
502   aldehydes butanal, 2-pentanone, and 2-heptanone with OH and NO_3 also leads to the formation of acetaldehyde,
503   sometimes with high yields (Atkinson et al., 2000). In the data presented here, acetaldehyde at 80 m correlated best
504   with photolytically generated species like MVK, methacrolein, and $C_5H_4O_3$ (p = 0.96) and with benzaldehyde
505   (p = 0.93) in the dry season and correlated well with acetic acid (p > 0.92) in both seasons. In the transition season
506   correlations were weaker overall (Figs. 3–4), which could hint at different primary and secondary acetaldehyde
507   sources. Correlation coefficients of acetaldehyde and BC at 325 m were below 0.6 at daytime but at nighttime, in the
508   transition season, a rather high correlation with p = 0.82 was observed (Fig. S5).

509   From about 16:00 LT onwards until the next day the vertical gradient is reversed with the lowest concentrations at
510   80 m. This likely reflects the uptake to plant tissues regulated by compensation points since the NO_3 and O_3 reactivity
511   is rather low. Acetaldehyde exhibits the strongest observed loss rate at nighttime among all the carbonyl compounds
512   in the dry season and it had the highest Henry's law constant (Table 2).

513   **4.2   Acetone**

514   Acetone (propanone) is the simplest ketone and the most abundant and widespread OVOC in the atmosphere due to
515   its relatively long atmospheric lifetime of 15 days (Singh et al., 2004) (primarily driven by photolysis in the upper
516   troposphere, 119 days with respect to OH). The variation of acetone mixing ratios throughout the day above the
517   roughness sublayer at 150 and 325 m was small compared to the other carbonyls. However, mixing ratios at 80 m
518   increased substantially with light and temperature during the day. In the wet–to–dry transition season mixing ratios
519   reached 1.33, 1.12, 1.15 ppb on average, while in the dry season, 2.55, 1.66, 1.71 ppb (80, 150, 325 m) were measured.

520   The vertical distribution of acetone showed clearly enhanced mixing ratios at 80 m during daytime compared to well-
521   mixed conditions at the higher sampling points. The gradient in the first 150 m above the canopy is strong despite the
522   low reactivity of acetone, which raised the question of how acetone is distributed vertically in the roughness sublayer.
523   Flux measurements in a tropical forest in Costa Rica in the dry season have found a bidirectional but net-positive
524   canopy flux of acetone (Karl et al., 2004). Additionally in 2013, when several carbonyls were measured at ATTO
525   below 80 m, the acetone mixing ratios inside the canopy (influenced by surrounding trees) were lower than the values

526 measured at 79 m in the dry season. Both studies deployed PTR-quadrupole-MS operated with H_3O^+ reagent ions with
527 a nominal mass resolution. As for acetaldehyde, these increasing vertical gradients suggested a dominance of
528 photolytically secondary formation over direct emission. In the wet season in 2013, however, mixing ratios measured
529 in the canopy and at 79 m were of similar magnitude and, compared to the dry season, much lower at both heights. In
530 conclusion, no clear dominance of secondary formation or direct emission was found in the wet season (Yáñez-Serrano
531 et al., 2015). We also observed seasonal differences at all three heights, with lower mixing ratios in the transition
532 compared to the dry season. While we cannot report acetone observations from the wet season, we did observe higher
533 correlations of acetone with non-primary emitted OVOC methacrolein, MVK, and $C_5H_4O_3$ in the transition season
534 (p > 0.82) compared to the dry season, suggesting that in 2019 secondary formation contributed more acetone to
535 observed mixing ratios in the transition season than in the dry season. In light of the widely differing atmospheric
536 lifetimes of acetone and those OVOC, the most likely explanations for the high transition season correlations is a
537 dominating secondary acetone source at a similar rate or similar surface uptake. Contributions from aged biomass
538 burning plumes containing acetone in the dry season, when enhanced BC concentrations were observed, could also be
539 the reason for a weaker correlation of $C_5H_4O_3$, methacrolein, and MVK with acetone in the dry season. Based on the
540 information obtained in 2013 and the observations from this study, secondary production in the dry and transition
541 season appears to peak above the canopy, adding up to varying contributions of direct emissions and uptake by
542 vegetation. It is thus possible that strong secondary formation competes with uptake by vegetation to generate a local
543 maximum in the rough surface layer, which is observed in this study by the enhanced mixing ratios observed at 80 m.
544 Sweeps and ejections in and out of the canopy in the roughness sublayer could make the uptake of acetone by different
545 vegetation species and soils very efficient. The strong gradient between 80 and 150 m likely reflects an acetone peak
546 in the vertical. In conclusion, the most relevant precursors were very reactive biogenic compounds. The best
547 correlations were found with MEK (p > 0.87) in both seasons, which is another long-lived ketone that is known to be
548 directly emitted from the Amazon rainforest and produced in the atmosphere overhead (Yáñez-Serrano et al., 2015,
549 2016).

550 Primary sources of acetone are direct emission from vegetation and, to a smaller extent, also from dead plant matter.
551 Acetone is released during cyanogenesis, which acts as a repellant that stops herbivores eating the plant's leaves.
552 During the production and release of volatile hydrogen cyanide, which deters the feeding herbivore, acetone is formed
553 as a byproduct. Cyanogenesis occurs in many plant species, though some employ different mechanisms to produce
554 hydrogen cyanide so that other carbonyl byproducts can be released (Fall, 2003). Another known biogenic pathway
555 for acetone formation is acetoacetate decarboxylation in soil bacteria and humans (Fall, 2003). Both light and
556 temperature have been suspected to drive acetone emissions, as shown for some pine and spruce trees (Seco et al.,
557 2007).

558 Secondary formation of acetone is known to occur from anthropogenically emitted C_3-C_5 isoalkanes (propane,
559 isobutane, isopentane) and biogenic emitted methyl butenol and certain terpenes (Fischer et al., 2014; Jacob et al.,
560 2002; Seco et al., 2007). We found mixing ratios of isopentane to be below the detection limit (13 ppt), and the vertical
561 distribution and correlations reported for acetone indicated a rapid formation in the rough surface layer by
562 hydrocarbons that are much more short-lived than alkanes. The ozonolysis of compounds in epicuticular leaf waxes
563 constitutes another source of acetone as mentioned in section 3.3.

564 At night, deposition could be observed on the basis of the rapidly decreasing mixing ratios at 80 m, compared to the
565 slowly occurring reactions with NO_3 and O_3. Similar effects have been reported in flux measurements performed by
566 Karl et al. (2004).

4.3 Propanal

568 Propanal is an isomer of acetone and is not distinguishable from acetone by classical PTR-MS type instruments using
569 H_3O^+. In this study, the first high temporal resolution measurements of propanal in a tropical forest are presented, and
570 the vertical distribution above the canopy was found to differ markedly from acetone. In general, in the remote
571 atmosphere, we may expect the more reactive propanal to have lower mixing ratios than acetone, although this may
572 not be true close to sources. We measured average concentrations of 176, 150, and 119 ppt in the wet–to–dry transition
573 and 165, 115, and 85 ppt in the dry season (80, 150, 325 m). The ratio of propanal to acetone in the roughness sublayer
574 of the tropical forest and above yields 1:7.6, 1:9.6 (transition season) and 1:15.4, 1:20 (dry season) at 80 and 325 m.

575 Globally, the mixing ratio of propanal has been estimated to be about one-third of acetaldehyde (Singh et al., 2004),
576 while at ATTO a ratio of 1:4.2, 1:8.1 (transition season) and 1:7.2, 1:14 (dry season) was measured at 80 and 325 m,
577 respectively. However, it should be noted that, globally, a large propanal source is propane oxidation, which is
578 predominantly emitted from anthropogenic activities associated with oil and gas use. Acetaldehyde sources in the
579 rainforest thus far exceed propanal sources in the context of the global budget (Warneck, P.; Williams, J., 2012).

580 Propanal emission from vegetation has been reported for non-tropical forests (Guenther, 2000; Villanueva-Fierro et
581 al., 2004), although the metabolic pathway was not specified. Wang et al. (2019) described the biosynthesis of
582 acetaldehyde and propanal during fruit ripening. It was also noted that propanal emission occurs from ferns (Isidorov
583 et al., 1985), which is important since fern species are common in the understory of tropical forests.

584 Throughout the day, propanal exhibited a negative vertical gradient (i.e., decreasing mixing ratio with increasing
585 height). This occurs most likely due to dilution and photochemical loss of propanal generated in or emitted from the
586 canopy. A similar distribution was also observed for monoterpenes and isoprene, which are primary emitted VOC.
587 Accordingly, propanal observed at 80 m also correlates best with isoprene in both seasons ($0.89 > p > 0.98$) followed
588 by monoterpenes ($0.84 > p > 0.92$). The estimated atmospheric lifetime of propanal of about 1 day (Guimbaud et al.,
589 2007) (1.2 days for the oxidation by OH, table 2) is similar to that of acetaldehyde, but the vertical profiles revealed
590 different distributions in the first 325 m above ground (Figures 1 and 2). The weak gradient of acetaldehyde between
591 150 and 325 m at daytime in contrast to the steadily decreasing vertical profile of propanal can thus only be explained
592 by a higher yield of acetaldehyde from secondary production above 150 m. This is not surprising since acetaldehyde
593 is produced during oxidative degradation of many hydrocarbons. The secondary production of propanal is known to
594 occur via the photochemical oxidation of C_3 and larger hydrocarbons (Singh et al., 2004) and propane (Altshuller,
595 1991). Their lifetimes range from 5 days to a few hours (Altshuller, 1991). However, due to the high correlation of
596 propanal and isoprene, which is even higher than the correlation of isoprene and its oxidation products MVK and
597 methacrolein, a primary and mainly light-dependent source is surmised.

598 Nighttime mixing ratios of propanal were decreasing at 80 m (Table 2). Since the reaction rate of propanal with NO_3
599 is faster and the water solubility lower than that of the other carbonyl compounds, a higher fraction could potentially
600 react in the atmosphere. Stomatal uptake for the terpenes might be driven by the concentration gradient between leaf
601 and atmosphere, and the same might hold for propanal.

4.4 Methyl Ethyl Ketone (MEK)

603 Mixing ratios of MEK in the wet–to–dry transition were 177, 175, and 177 ppt on average, compared to 249, 188, and
604 185 ppb in the dry season (80, 150, 325 m). With a conventional PTR-MS, butanal and MEK are detected at the same
605 exact mass, whereas in this study using NO^+ reagent ions solely MEK was measured. Butanal mixing ratios were
606 determined to be below the detection limit (20 ppt); thus, the contribution of butanal to MEK for PTR-MS can be
607 assumed to be very low. The mixing ratios obtained in this study agree well with previous studies conducted with a
608 PTR-quadrupole-MS at the ATTO site in 2013 and close to Manaus (Amazonia) in 2014, which would not completely
609 exclude possible interferences on the nominal mass of MEK (Yáñez-Serrano et al., 2015, 2016). The vertical
610 distribution of MEK throughout the day resembles that of acetone in both seasons. Mixing ratios above the roughness
611 layer (at 150 and 325 m) were almost uniform, while those at 80 m showed a more pronounced diurnal cycle with
612 strongly increasing values in the day and decreasing values at night. As well as being structurally similar to acetone,
613 MEK also has a long lifetime of 4.3 days (Fischer et al., 2014) (19.3 with respect to OH oxidation alone) relative to
614 mixing timescales. MEK is also known to have primary and secondary sources (Yáñez-Serrano et al., 2016) and to be
615 uptaken by vegetation (Edtbauer et al., 2021; Tani et al., 2013). Therefore, it is not surprising that MEK correlated
616 best with acetone at 80 m ($p = 0.87$ in the dry season), but in the transition season, it also correlated well with $C_5H_4O_3$,
617 methacrolein, and MVK. This suggests secondary sources from biogenically emitted precursors were more dominant
618 during the transition season than in the dry season, similar to acetone.

619 MEK emissions have been reported for rainforest canopies (Yáñez-Serrano et al., 2015) and fern (Isidorov et al.,
620 1985), decaying plant matter (Warneke et al., 1999), fungi, and bacteria (Yáñez-Serrano et al., 2016). The metabolic
621 pathways of production and the release mechanisms are poorly understood but have been suggested to involve plant
622 signaling, injured leaves, and root-aphid interactions (Yáñez-Serrano et al., 2016). Within-plant conversion of the

623 cytotoxic 1,2-ISOPOOH, which was deposited on poplar leaves, first to MVK and subsequently to MEK, has been
624 reported to represent a large biogenic source of MEK. The enzyme responsible for the conversion of MVK to MEK
625 is widespread among plants (Canaval et al., 2020).

626 The secondary formation of MEK occurs via the oxidation of n-butane with a yield of 80% (Singh et al., 2004) and
627 via oxidation of 2-butanol, 3-methyl pentane, and 2-methyl-1-butene (Yáñez-Serrano et al., 2016). Additionally, all
628 alkenes with a methyl/ethyl group on the same side of the olefin bond are possible precursors of MEK (Singh et al.,
629 2004). Butane was not expected to be abundant in the rainforest environment due to its anthropogenic sources, and
630 butane oxidation would also yield butanal, which was only detected below the LOD. As for acetone, the vertical
631 distribution and correlations discussed above suggest higher levels of short-lived precursors of MEK than of alkanes.

632 Rapidly decreasing concentrations at 80 m at night are in agreement with earlier studies, that reported deposition of
633 MEK in the canopy due to its high water solubility (Yáñez-Serrano et al., 2016) (Table 2).

4.5   Methyl Vinyl Ketone and Methacrolein/2-Butenal

635 The main source of both carbonyls MVK and methacrolein is the oxidation of isoprene by OH. Thus, they are
636 summarized in one section. It has been shown previously that methacrolein is detected together with 2-butenal (Koss
637 et al., 2016), which is also found in vegetation emission studies, albeit in small concentrations (Hellén et al., 2004;
638 Isidorov et al., 1985). (E)-2-butenal is a signaling compound within the plant that serves to trigger responses to abiotic
639 stress (Yamauchi et al., 2015). Its atmospheric lifetime is around 20 hours, slightly longer than the lifetimes of
640 methacrolein and MVK which are 10 and 14 hours, respectively (Hellén et al., 2004; Liu et al., 2016). It is also known
641 that MVK and methacrolein cannot be detected separately from isoprene hydroxyhydroperoxides (ISOPOOH) without
642 using a scrubber, since the hydroperoxides decompose onto the same m/z. With NO^+ CIMS the fragment of 1,2-
643 ISOPOOH and methacrolein share one m/z-ratio, while 4,3-ISOPOOH is detected together with MVK (Rivera-Rios
644 et al., 2014). Wall exchange effects in the inlet line might have led to the removal of ISOPOOH from the sampled air
645 due to their reduced volatility, but a contribution to the MVK and methacrolein signal remains possible. ISOPOOH
646 also originate from the oxidation of isoprene and are very reactive, reflected by lifetimes of 3 and 2 hours. After the
647 initial reaction of OH and isoprene, the subsequently formed peroxy radical (RO_2) can react with NO to form MVK
648 and methacrolein, but it can also react with HO_2 to form ISOPOOH (Liu et al., 2016). At close to pristine conditions
649 at ATTO, NO mixing ratios are low, and the yield distribution between ISOPOOH, MVK, and methacrolein was
650 estimated to be 50, 25, and 25%, respectively (Ringsdorf et al., 2023; Rivera-Rios et al., 2014). It has been shown that
651 the oxidation of isoprene can proceed already within plant tissues by reaction with accumulated reactive oxygen
652 species. The accumulation of reactive oxygen species, including OH, is a reaction to biotic and abiotic stresses and
653 can exceed the antioxidant defense capacities in the tissue. The oxidation of isoprene within the tissue reduces the
654 amount of reactive oxidized species and leads to the direct emission of isoprene's products MVK and methacrolein,
655 especially under stress (Jardine et al., 2012b, 2013).

656 Oxidation of the monoterpene ocimene has been identified as another secondary source for MVK (Calogirou et al.,
657 1999). To our knowledge, there are no other significant direct or secondary sources of MVK, methacrolein, and
658 ISOPOOH other than the oxidation of isoprene. This explains the observed diurnal cycle with an afternoon maximum
659 due to the light-dependent emission of isoprene and the photochemical production of OH. Since isoprene is present at
660 relatively high mixing ratios at all tree sampling heights (3.69, 3.33, 3.0 ppb at 80, 150, and 325 m in the dry season),
661 the oxidative formation of MVK, methacrolein, and ISOPOOH takes place throughout the mixed layer. The observed
662 slightly increasing mixing ratios of MVK with height are consistent with rapid isoprene oxidation above the canopy,
663 slower removal of MVK itself, and turbulent in-mixing of cleaner air from above. Isoprene has an estimated
664 atmospheric lifetime of about 3 hours, and it was previously reported that only circa 10% of emitted isoprene was
665 oxidized within the canopy (Karl et al., 2004). Unlike MVK, methacrolein and 2-butenal show a slightly decreasing
666 vertical gradient. Sources and sinks of MVK and methacrolein are very closely related, so the presence of significant
667 quantities of 2-butenal is the most likely explanation for that difference.

668 Dry deposition to leaf surfaces has been observed in a previous study for the sum of MVK and methacrolein and
669 individually for these compounds during daytime (Nguyen et al., 2015; Tani et al., 2010). Uptake by leaves represents

670 a significant sink that exceeds loss via OH oxidation near leaves (Tani et al., 2010). In this study, the rapid decrease
671 of nocturnal concentrations at 80 m indicated that deposition at night was also taking place.

672 MVK and methacrolein + 2-butenal showed similar mixing ratios in the dry season of 607, 599, 659 ppt MVK and
673 679, 644, 644 ppt methacrolein + 2-butenal. It has to be considered that the uncertainty of MVK mixing ratios is higher
674 than the uncertainty of methacrolein mixing ratios due to their k-rate-based calculation rather than calibration to a gas
675 standard. In the transition season, methacrolein + 2-butenal (415, 425, 439 ppt) exceeded the mixing ratios of MVK
676 (184, 229, 265 ppt). Whether that resulted from the high seasonal variability of 2-butenal or from the contribution of
677 ISOPOOH, unfortunately, remains unclear. Lower levels of all isoprene oxidation products were expected as a result
678 of lower isoprene mixing ratios and photo-oxidation rates in the transition season.

679 **4.6   Sum of C_5-ketones**

680 The mixing ratios obtained for the sum of C_5-ketones were 11, 9, and 9 ppt in the transition season, while slightly
681 higher levels of 14, 8, and 7 ppt (80, 150, 325 m) were obtained in the dry season. A diurnal cycle was observed at
682 80 m only, whereas levels at 150 and 325 m were similar and showed no trend throughout the day and night. C_5-
683 ketones were 2- and 3- pentanone as well as 3-methyl-2-butanone. The atmospheric lifetime of 2-pentanone is in the
684 range of 5 days. All three ketones have been included in emission inventories from plants (Isidorov et al., 1985;
685 Kesselmeier and Staudt, 1999; König et al., 1995), but there is little information on metabolic pathways or
686 mechanisms. 2-pentanone has been identified as a marker for fungal activity in indoor environments (Kalalian et al.,
687 2020), since it is produced in the hyphae of *Aspergillus niger* (Lewis, 1970), a fungus that was also found to degrade
688 biomass in the Amazon. 3-pentanone is one of the C_5 green leaf volatiles (GLV) emitted at lower rates than C_6 GLV,
689 which are described in the next section (Jardine et al., 2012a). An increase of 3-pentanone coincident with high
690 temperatures after noon was observed at another measurement station in the Amazon rainforest, with a simultaneous
691 decrease of terpenoid emissions (Jardine et al., 2015). Consistent with this observation, in this study, the correlation
692 of C_5 ketones with isoprene or monoterpenes was low in the transition and dry season during the daytime ($p < 0.39$).
693 The best correlations for C_5-ketones of $0.53 < p < 0.6$ were obtained with acetone and MEK. This was most likely a
694 consequence of common sources, including primary emission and formation from rather short-lived hydrocarbons and
695 of the long atmospheric lifetimes relative to mixing timescales, which the observed ketones have in common. Above
696 150 m, no diurnal variability was observed, which is also in agreement with the other ketones, suggesting they were
697 well-mixed above the Amazonian roughness sublayer. As suspected for acetone, the vertical distribution of C_5-ketones
698 might have been peaking around 80 m as a result of the bidirectional exchange in the canopy and secondary formation.

699 Fumigation experiments with different VOC have shown a loss of all three C_5-ketones on leaf surfaces (Tani and
700 Hewitt, 2009). A decrease of the mixing ratios at 80 m could be observed at nighttime, and a high water solubility of
701 the ketones indicated a high loss rate. However, the signal was too noisy to determine loss rates from the data.

702 C_5-aldehydes, which were usually detected together with the C_5-ketones, exhibited lower mixing ratios, especially in
703 the dry season. Overall, the mixing ratios were below their LOD and thus not investigated in detail. However, a diurnal
704 and vertical pattern of C_5-aldehydes with vertical and diurnal variabilities different to those of the C_5-ketones was still
705 apparent.

706

707 **4.7   n-Hexanal/Hexenols and Hexenals**

708 C_6-aldehydes, namely n-hexanal, Z-2-hexenal, Z-3-hexenal, E-2-hexenal, and E-3-hexenal, together with C_6-alcohols
709 and esters form a group that is often termed green leaf volatiles (GLV). Although different temporal variabilities were
710 observed for n-hexanal/hexenols and hexenals, we here discuss them together in one section due to their common
711 sources.

712 In the chloroplasts of almost all green plants, GLV are synthesized from fatty acids as part of the oxylipin pathway.
713 Their emission results from wounding or mechanical damage, from abiotic factors (such as wind), herbivores, and
714 pathogen attack (Scala et al., 2013). The amount of GLV emitted from corn plants has been shown to depend on soil
715 water content, temperature, light, and fertilization, with a stronger emission response at higher temperatures

(Gouinguené and Turlings, 2002). Furthermore, emission has been reported as a response to abiotic stress from light–dark transitions (Jardine et al., 2012a). Their production and release can be very fast; in the case of Z-3-hexenal, emission begins only 1 or 2 seconds after damage (Fall et al., 1999). On one hand, GLV have antibiotic properties and protect the wounded tissue from invading bacteria or other microorganisms. On the other hand, their rapid production and release make them useful for intra and inter-chemical communication in plants, for example for priming defense mechanisms. It has been found that a herbivore-infested plant releases signaling compounds, like GLV to attract the predator (insects, beetles, birds, etc.) of the herbivore (Mumm and Dicke, 2010; Scala et al., 2013; Zannoni et al., 2020a). The release of GLV can happen on short timescales of minutes to hours but in cases of repetitive wounding or drying of leaves, the emission can be continuous over days (Fall et al., 1999; Scala et al., 2013). Release of GLV is also caused by drought stress, and GLV levels have been observed to increase at noon as a result of high temperatures in the Amazon forest (Jardine et al., 2015; Kesselmeier and Staudt, 1999).

It remains unclear if the leaf alcohol Z-3-hexanol contributed to the hexanal signal. Z-3-hexanol is also a GLV and has been reported to represent a major part of the emission of many studied plants (Kesselmeier and Staudt, 1999). Its atmospheric lifetime was calculated to be 5 hours with respect to OH. Further, the less abundant isomers, such as Z-4-hexenol or E-2-hexenol, are also likely to contribute to the hexanal signal. Due to photolysis and reaction with OH, the lifetime of n-hexanal is about 4 hours (12 hours for oxidation by OH only), which is also true for E-2-hexenal (Jiménez et al., 2007). Z-3-hexenal has a shorter atmospheric lifetime of 3 hours (Xing et al., 2012).

At ATTO, the integrated emissions from a large uniform area were measured, which made it impossible to detect single wounding events, except for large-scale storm damage or human activities such as forest clearing. Measured mixing ratios were 15, 11, and 9 ppt for n-hexanal in the transition season and 26, 19, and 16 ppt in the dry season. Hexenals were detected at mixing ratios below LOD (6 ppt) for most parts of the day in the transition season, and 8 ppt were measured at 80 m in the dry season. Nighttime mixing ratios of hexenals at 150 and 325 m were, however, also below the LOD (6 ppt). During both measurement phases, n-hexanal was continuously present, exhibiting a distinct diurnal cycle with maximum mixing ratios in the afternoon and higher values in the dry season. Since the emission rate of damaged leaves of hexenals was found to be higher compared to n-hexanal (Fall et al., 1999), the contribution of hexenols to the signal of n-hexanal was very likely. Average daytime mixing ratios between 40 and 70 ppt have also been observed for hexanal and/or hexenols in an elevated position above the rainforest of Malaysia (Langford et al., 2010). To investigate whether the diurnal cycle results from temperature-dependent emission of GLV or additional secondary formation, measurements inside the canopy are required.

It was not surprising that a continuous decrease in both n-hexanal and hexenols with height was observed throughout the day, similar to propanal and other reactive primary emissions like isoprene and monoterpenes. Correlations at 80 m with isoprene ($0.78 < p < 0.86$), monoterpenes ($0.74 < p < 0.91$), and propanal ($p = 0.88$, dry season) indicated light- or temperature-driven emission or rapid secondary formation close to the canopy. This correlation is interesting since GLV emissions upon biotic-induced stresses such as herbivory do not necessarily follow a diel cycle. However, boundary layer dynamics might have modulated the diel cycle since mixing between the canopy and atmosphere is most efficient during daytime convective conditions. Additionally, temperature-related drying of leaves could have led to the observed diel variability.

In contrast to n-hexanal/hexenols, hexenals exhibit a more pronounced seasonal variability, with very low mixing ratios, mostly below the LOD, in the transition season. The correlation with isoprene and monoterpenes during the daytime in the dry season was rather low ($p = 0.71$), with the highest correlations for acetone, MEK, benzaldehyde, and ethanol ($p > 0.8$), suggesting primary and secondary sources of hexenals.

For all C_6-aldehydes investigated in this section, decreasing concentrations during nighttime at all three heights were observed in the dry season, when C_6-aldehydes mixing ratios were generally higher than in the transition season. A slightly slower decrease of 80-m mixing ratios compared to the higher levels in the dry season may indicate a continued nocturnal emission of GLV, which is plausible since production and release from mechanical wounding, stress, or herbivory is possible without light (He et al., 2021).

4.8 Benzaldehyde

The average mixing ratios of benzaldehyde measured in this study are 12, 12, 12 ppt in the transition season and 11, 10, 11 ppt (80, 150, 325 m) in the dry season. No seasonal variability or vertical gradient was observed between the measurement periods.

Benzaldehyde is the lightest monoaromatic aldehyde and is formed via the oxidation of other aromatic compounds. It is a major intermediate product of the oxidation of benzyl radicals via OH and, thereby, of all alkyl-substituted aromatic hydrocarbons (Sebbar et al., 2011). Biogenic aromatics, such as volatile benzenoids or larger molecules like lignols, are produced via the shikimate pathway by plants, which is an important metabolic process, but benzaldehyde can also be emitted by microorganisms (Ladino-Orjuela et al., 2016; Laothawornkitkul et al., 2009). The oxidation of toluene, which has previously been observed to be emitted from forested environments and farm crops (Heiden et al., 1999), yields benzaldehyde as a product (6-%) (Atkinson and Arey, 2003). Benzaldehyde is also a benzyl alcohol oxidation product, which has been reported previously to be emitted from biogenic sources (Bernard et al., 2013). Benzaldehyde is very reactive, with a calculated atmospheric lifetime primarily determined by its photolysis rate of 2.4 hours (Cabrera-Perez et al., 2016) (1.7 days with respect to OH).

Primary emission of benzaldehyde from vegetation has been reported for grass (Kirstine et al., 1998) and elevated concentrations under and within the canopy of the Amazon rainforest were measured (Kesselmeier et al., 2000). The high mixing ratios (about 300 ppt) found at the ground were suspected to result from the decomposition of biomass, specifically the decomposition of lignols within the litter. In that study, the mixing ratios above the canopy were much lower than those measured at ground level.

The apparent light or temperature-driven diurnal cycle of benzaldehyde suggests secondary photochemical production from aromatic hydrocarbons, as the shikimate pathway is independent of light (Jan et al., 2021). The atmospheric lifetime of precursor aromatics ranges from days to weeks (Altshuller, 1991). Secondary production from long-lived precursors is a feasible explanation for the missing vertical variability of the very reactive benzaldehyde in the first 325 m of the mixed layer. The rather slow secondary production throughout the mixed layer possibly compensated for the expected loss through oxidation and dilutive mixing. Mixing ratios observed at 80 m were only slightly more abundant in the dry season compared to higher altitudes, which could mean a stronger contribution of benzaldehyde emissions. However, the narrow vertical benzaldehyde distribution points towards well-mixed aromatic precursor hydrocarbons. Daytime mixing ratios of carbonyls that are suspected to be formed predominantly due to photochemical formation, namely, acetic acid, $C_5H_4O_3$, methacrolein, MVK, but also acetaldehyde and acetone, correlate very well with benzaldehyde in the dry season ($0.85 > p > 0.95$). In the transition season, the correlation with the same compounds is smaller ($0.75 > p > 0.86$). Possible explanations for this difference most likely lie in altered sources of precursors or benzaldehyde itself due to differences in, e.g., litter decomposing activities. It is important to note that the missing vertical variability could also be a sign of contamination from the measurement tower itself, e.g., through temperature-dependent outgassing of its coating. However, the measurement of the fresh paint did not show elevated benzaldehyde, while the fresh anticorrosion agent emits some benzaldehyde, but at much lower rates than other VOC, e.g., toluene or xylene.

Globally, dry deposition constitutes a small sink of benzaldehyde in the same range as oxidation by NO_3 (Cabrera-Perez et al., 2016). We observed decreasing mixing ratios at all three heights throughout the night (Table 2). Wet deposition and uptake to leaves and soil might have been the dominant sink.

There is evidence that benzaldehyde PAN can emerge when transported to high NOx regions (Caralp et al., 1999). Mixing ratios of PAN are quite high so this must be considered, but photochemical PAN creation potential is the lowest of the whole group of organic compounds (Derwent et al., 1998).

5   Conclusion

In this study, a PTR-ToF-MS was operated using NO^+ as the reagent ion for measuring specific carbonyl compounds at three heights (80, 150, 325 m), in two seasons, and over 24-hour cycles, on the ATTO tower located in the Brazilian Amazon rainforest. With the more commonly used ionization method for PTR-MS involving H_3O^+ ions, aldehyde and ketone isomers were detected together at the same exact mass. This precludes the investigation of the individual species. For the first time, mixing ratios of biogenic aldehydes and ketones measured at high frequency are reported for a rainforest ecosystem. Generally, higher mixing ratios were found in the dry season. To some extent, this can be attributed to higher temperatures and enhanced light conditions, which drive emissions and photochemical activity. However, since temperature and PAR were only slightly enhanced in the dry season compared to the wet–to–dry transition, other aspects such as phenology (gross ecosystem productivity peaking in the dry season) and contribution of long-lived species from aged biomass burning plumes are of importance. Ketones have atmospheric lifetimes (days to weeks) that are much longer than the vertical mixing times (15–60 min) (Ringsdorf et al., 2023). Such compounds can, therefore, be expected to be also present above the lowermost mixing layer (ABL) in the residual layer and free troposphere. Interestingly, elevated ketone mixing ratios in the roughness sublayer observed at 80 m by day suggest a large source above or at canopy level, balanced with a surface uptake process. To examine these strong vertical gradients observed for some ketones, continuous measurements with altitude are planned using a PTR-ToF-MS installed on an elevator attached to the tower. This system will allow investigation of the exchange of VOC between canopy and atmosphere and reveal whether mixing ratios of acetone, MEK and C_5-ketones are peaking around 80 m as suggested by the observed elevated mixing ratios at 80 m. At night, the loss of these species indicates a rapid deposition to the canopy or the underlying forest floor. The correlations shown in Figures 3–4 reveal seasonal differences in the partitioning of primary emission from the canopy and the rate of rapid secondary production above the canopy. The most abundant individually measured carbonyls in this study were acetaldehyde and acetone, both effective PAN precursors, followed by isoprene oxidation products and propanal. Note that formaldehyde was not detected by the applied method. The shorter-lived, longer-chain aldehydes observed in this study showed great variation, exhibiting both increasing and decreasing vertical gradients that vary considerably in strength. All carbonyl compounds showed a distinct diurnal cycle which followed the evolution of light and temperature during the day and, for most compounds, a decrease during the night driven in part by reaction with NO_3 but more importantly by deposition to plant tissues, as has been shown by flux measurements for a few oxygenated species before (Karl et al., 2004). The nocturnal uptake of these carbonyl compounds is an important aspect of their local-to-regional-scale budget. Based on this data, we hypothesize that the ecosystem can more efficiently produce reduced species such as isoprene and monoterpenes but more efficiently utilize the oxygenated products of these precursors. The importance of uptake followed by metabolization or storage, especially for oxygenated BVOC has been stressed already in the context of bidirectional exchange of BVOC by Niinemets et al. (2014). This would imply that the rainforest exploits atmospheric oxidation to convert products into more useful, metabolizable forms. Similar preferences for the uptake of oxygenated species over terpenes have been reported for epiphytes such as lichen and moss (Edtbauer et al., 2021). This idea can serve as the basic hypothesis for future plant experiments and the observed loss rates of carbonyl species can help to constrain turbulence resolving canopy exchange models. Overall, we need to improve our understanding of the complexity of biological production and consumption and invest into investigations of primary emissions on a leaf or branch level.

Butanal, and carbonyls higher than C_7 were found to be minor components of the rainforest atmosphere, as were the alkanes isopentane, methylcyclopentane, sum of 2- and 3-methylpentane and C_7 cyclic alkanes. The ratio of the aldehydes propanal and acetaldehyde, which have comparable atmospheric lifetimes and which were shown to correlate very well in previous studies, was found to be much higher with 1:4.2 and 1:7.2 in the transition and dry season at 80 m compared to the global average ratio of 1:3 (Singh et al., 2004), due to the overwhelming predominance of biogenic sources and precursors in the rainforest.

This application of the NO^+ CIMS method has enabled the study of the individual carbonyls not accessible using the H_3O^+-based method. We, therefore, recommend periodic switching of the reagents to allow for more specific detection of biogenic emissions. This would complement long-term measurements conducted using the H_3O^+ ionization method.

854 **Code availability.** The python code can be provided upon request.

855 **Data availability.** BVOC datasets are available on the ATTO data portal (https://doi.org/10.17871/atto.355.4.1493,
856 https://doi.org/10.17871/atto.354.3.1494, https://doi.org/10.17871/atto.353.7.1495, and
857 https://doi.org/10.17871/atto.352.7.1496). Meteorological data conducted at the ATTO tower (320 m) in 2019 are
858 available via https://doi.org/10.17871/atto.95.12.742.

859 **Supplement link**: A link to the supplement will be included by Copernicus, if applicable.

860 **Author contributions**: AR and AE conducted the BVOC measurements and AR analyzed this data and drafted the
861 manuscript. BH and CP provided the black carbon observations and meteorological parameters conducted at the
862 325–m–tall tower. MOS and AA conducted the measurements of the meteorological parameters at the 80 m tower.
863 J.W. supervised this study. J.L. supervised the research that led to this study.

864 **Competing interests**: The authors declare that they have no conflict of interest.

865 **Acknowledgements:** We acknowledge the support by the German Federal Ministry of Education and Research
866 (BMBF contract 01LB1001A and 01LK1602B) and the Brazilian Ministério da Ciência, Tecnologia e Inovação
867 (MCTI/FINEP contract 01.11.01248.00) as well as the Amazon State University (UEA), FAPESP, CNPq, FAPEAM,
868 LBA/INPA, and SDS/CEUC/RDS-Uatumã. We thank Thomas Klüpfel for his help with VOC measurements. We
869 especially acknowledge the technical and logistical support of the ATTO team (in particular Reiner Ditz and Hermes
870 Braga Xavier). We also thank Andrew Crozier for creating and providing a detailed map of the ATTO site.

6   References

872 Altshuller, A. P.: Chemical reactions and transport of alkanes and their products in the troposphere, J. Atmospheric
873 Chem., 12, 19–61, https://doi.org/10.1007/BF00053933, 1991.

874 Andreae, M. O.: Emission of trace gases and aerosols from biomass burning – an updated assessment, Atmospheric
875 Chem. Phys., 19, 8523–8546, https://doi.org/10.5194/acp-19-8523-2019, 2019.

876 Andreae, M. O. and Merlet, P.: Emission of trace gases and aerosols from biomass burning, Glob. Biogeochem.
877 Cycles, 15, 955–966, https://doi.org/10.1029/2000GB001382, 2001.

878 Andreae, M. O., Artaxo, P., Brandão, C., Carswell, F. E., Ciccioli, P., da Costa, A. L., Culf, A. D., Esteves, J. L.,
879 Gash, J. H. C., Grace, J., Kabat, P., Lelieveld, J., Malhi, Y., Manzi, A. O., Meixner, F. X., Nobre, A. D., Nobre, C.,
880 Ruivo, M. d. L. P., Silva-Dias, M. A., Stefani, P., Valentini, R., von Jouanne, J., and Waterloo, M. J.: Biogeochemical
881 cycling of carbon, water, energy, trace gases, and aerosols in Amazonia: The LBA-EUSTACH experiments, J.
882 Geophys. Res. Atmospheres, 107, LBA 33-1-LBA 33-25, https://doi.org/10.1029/2001JD000524, 2002.

883 Andreae, M. O., Acevedo, O. C., Araùjo, A., Artaxo, P., Barbosa, C. G. G., Barbosa, H. M. J., Brito, J., Carbone, S.,
884 Chi, X., Cintra, B. B. L., da Silva, N. F., Dias, N. L., Dias-Júnior, C. Q., Ditas, F., Ditz, R., Godoi, A. F. L., Godoi,
885 R. H. M., Heimann, M., Hoffmann, T., Kesselmeier, J., Könemann, T., Krüger, M. L., Lavric, J. V., Manzi, A. O.,
886 Lopes, A. P., Martins, D. L., Mikhailov, E. F., Moran-Zuloaga, D., Nelson, B. W., Nölscher, A. C., Santos Nogueira,
887 D., Piedade, M. T. F., Pöhlker, C., Pöschl, U., Quesada, C. A., Rizzo, L. V., Ro, C.-U., Ruckteschler, N., Sá, L. D. A.,
888 de Oliveira Sá, M., Sales, C. B., dos Santos, R. M. N., Saturno, J., Schöngart, J., Sörgel, M., de Souza, C. M., de
889 Souza, R. A. F., Su, H., Targhetta, N., Tóta, J., Trebs, I., Trumbore, S., van Eijck, A., Walter, D., Wang, Z., Weber,
890 B., Williams, J., Winderlich, J., Wittmann, F., Wolff, S., and Yáñez-Serrano, A. M.: The Amazon Tall Tower
891 Observatory (ATTO): overview of pilot measurements on ecosystem ecology, meteorology, trace gases, and aerosols,
892 Atmospheric Chem. Phys., 15, 10723–10776, https://doi.org/10.5194/acp-15-10723-2015, 2015.

893 Atkinson, R. and Arey, J.: Atmospheric Degradation of Volatile Organic Compounds, Chem. Rev., 103, 4605–4638,
894 https://doi.org/10.1021/cr0206420, 2003.

895   Atkinson, R., Tuazon, E. C., and Aschmann, S. M.: Atmospheric Chemistry of 2-Pentanone and 2-Heptanone,
896   Environ. Sci. Technol., 34, 623–631, https://doi.org/10.1021/es9909374, 2000.

897   Bernard, F., Magneron, I., Eyglunent, G., Daële, V., Wallington, T. J., Hurley, M. D., and Mellouki, A.: Atmospheric
898   Chemistry of Benzyl Alcohol: Kinetics and Mechanism of Reaction with OH Radicals, Environ. Sci. Technol., 47,
899   3182–3189, https://doi.org/10.1021/es304600z, 2013.

900   Bond, D. W., Steiger, S., Zhang, R., Tie, X., and Orville, R. E.: The importance of NOx production by lightning in
901   the tropics, Atmos. Environ., 36, 1509–1519, https://doi.org/10.1016/S1352-2310(01)00553-2, 2002.

902   Bourtsoukidis, E., Behrendt, T., Yañez-Serrano, A. M., Hellén, H., Diamantopoulos, E., Catão, E., Ashworth, K.,
903   Pozzer, A., Quesada, C. A., Martins, D. L., Sá, M., Araujo, A., Brito, J., Artaxo, P., Kesselmeier, J., Lelieveld, J., and
904   Williams, J.: Strong sesquiterpene emissions from Amazonian soils, Nat. Commun., 9, 2226,
905   https://doi.org/10.1038/s41467-018-04658-y, 2018.

906   Bracho-Nunez, A., Knothe, N. M., Costa, W. R., Maria Astrid, L. R., Kleiss, B., Rottenberger, S., Piedade, M. T. F.,
907   and Kesselmeier, J.: Root anoxia effects on physiology and emissions of volatile organic compounds (VOC) under
908   short-and long-term inundation of trees from Amazonian floodplains, SpringerPlus, 1, 9, https://doi.org/10.1186/2193-
909   1801-1-9, 2012.

910   Breuninger, C., Meixner, F. X., and Kesselmeier, J.: Field investigations of nitrogen dioxide (NO_2) exchange between
911   plants and the atmosphere, Atmospheric Chem. Phys., 13, 773–790, https://doi.org/10.5194/acp-13-773-2013, 2013.

912   Brown, S. S. and Stutz, J.: Nighttime radical observations and chemistry, Chem. Soc. Rev., 41, 6405,
913   https://doi.org/10.1039/c2cs35181a, 2012.

914   Cabrera-Perez, D., Taraborrelli, D., Sander, R., and Pozzer, A.: Global atmospheric budget of simple monocyclic
915   aromatic compounds, Atmospheric Chem. Phys., 16, 6931–6947, https://doi.org/10.5194/acp-16-6931-2016, 2016.

916   Calogirou, A., Larsen, B. R., and Kotzias, D.: Gas-phase terpene oxidation products: a review, Atmos. Environ., 33,
917   1423–1439, https://doi.org/10.1016/S1352-2310(98)00277-5, 1999.

918   Canaval, E., Millet, D. B., Zimmer, I., Nosenko, T., Georgii, E., Partoll, E. M., Fischer, L., Alwe, H. D., Kulmala, M.,
919   Karl, T., Schnitzler, J.-P., and Hansel, A.: Rapid conversion of isoprene photooxidation products in terrestrial plants,
920   Commun. Earth Environ., 1, 1–9, https://doi.org/10.1038/s43247-020-00041-2, 2020.

921   Cappellin, L., Karl, T., Probst, M., Ismailova, O., Winkler, P. M., Soukoulis, C., Aprea, E., Märk, T. D., Gasperi, F.,
922   and Biasioli, F.: On Quantitative Determination of Volatile Organic Compound Concentrations Using Proton Transfer
923   Reaction Time-of-Flight Mass Spectrometry, Environ. Sci. Technol., 46, 2283–2290,
924   https://doi.org/10.1021/es203985t, 2012.

925   Caralp, F., Foucher, V., Lesclaux, R., Wallington, T. J., and Hurley, M. D.: Atmospheric chemistry of benzaldehyde:
926   UV absorption spectrum and reaction kinetics and mechanisms of the C6H5C(O)O2 radical, Phys. Chem. Chem.
927   Phys., 1, 3509–3517, https://doi.org/10.1039/a903088c, 1999.

928   Chamecki, M., Freire, L. S., Dias, N. L., Chen, B., Dias-Junior, C. Q., Machado, L. A. T., Sörgel, M., Tsokankunku,
929   A., and Araújo, A. C. de: Effects of Vegetation and Topography on the Boundary Layer Structure above the Amazon
930   Forest, J. Atmospheric Sci., 77, 2941–2957, https://doi.org/10.1175/JAS-D-20-0063.1, 2020.

931   Chaparro-Suarez, I. G., Meixner, F. X., and Kesselmeier, J.: Nitrogen dioxide (NO2) uptake by vegetation controlled
932   by atmospheric concentrations and plant stomatal aperture, Atmos. Environ., 45, 5742–5750,
933   https://doi.org/10.1016/j.atmosenv.2011.07.021, 2011.

934   Chen, Y., Yuan, B., Wang, C., Wang, S., He, X., Wu, C., Song, X., Huangfu, Y., Li, X.-B., Liao, Y., and Shao, M.:
935   Online measurements of cycloalkanes based on NO[+] chemical ionization in proton transfer reaction time-of-flight

936   mass spectrometry (PTR-ToF-MS), Atmospheric Meas. Tech., 15, 6935–6947, https://doi.org/10.5194/amt-15-6935-
937   2022, 2022.

938   Chevuturi, A., Klingaman, N. P., Rudorff, C. M., Coelho, C. A. S., and Schöngart, J.: Forecasting annual maximum
939   water level for the Negro River at Manaus, Clim. Resil. Sustain., 1, e18, https://doi.org/10.1002/cli2.18, 2022.

940   Ciccioli, P., Silibello, C., Finardi, S., Pepe, N., Ciccioli, P., Rapparini, F., Neri, L., Fares, S., Brilli, F., Mircea, M.,
941   Magliulo, E., and Baraldi, R.: The potential impact of biogenic volatile organic compounds (BVOCs) from terrestrial
942   vegetation on a Mediterranean area using two different emission models, Agric. For. Meteorol., 328, 109255,
943   https://doi.org/10.1016/j.agrformet.2022.109255, 2023.

944   Colomb, A., Williams, J., Crowley, J., Gros, V., Hofmann, R., Salisbury, G., Klüpfel, T., Kormann, R., Stickler, A.,
945   Forster, C., and Lelieveld, J.: Airborne Measurements of Trace Organic Species in the Upper Troposphere Over
946   Europe: the Impact of Deep Convection, Environ. Chem., 3, 244–259, https://doi.org/10.1071/EN06020, 2006.

947   Deming, B. L., Pagonis, D., Liu, X., Day, D. A., Talukdar, R., Krechmer, J. E., de Gouw, J. A., Jimenez, J. L., and
948   Ziemann, P. J.: Measurements of delays of gas-phase compounds in a wide variety of tubing materials due to gas–
949   wall interactions, Atmospheric Meas. Tech., 12, 3453–3461, https://doi.org/10.5194/amt-12-3453-2019, 2019.

950   Derwent, R. G., Jenkin, M. E., Saunders, S. M., and Pilling, M. J.: Photochemical ozone creation potentials for organic
951   compounds in northwest Europe calculated with a master chemical mechanism, Atmos. Environ., 32, 2429–2441,
952   https://doi.org/10.1016/S1352-2310(98)00053-3, 1998.

953   Edtbauer, A., Pfannerstill, E. Y., Pires Florentino, A. P., Barbosa, C. G. G., Rodriguez-Caballero, E., Zannoni, N.,
954   Alves, R. P., Wolff, S., Tsokankunku, A., Aptroot, A., de Oliveira Sá, M., de Araújo, A. C., Sörgel, M., de Oliveira,
955   S. M., Weber, B., and Williams, J.: Cryptogamic organisms are a substantial source and sink for volatile organic
956   compounds in the Amazon region, Commun. Earth Environ., 2, 1–14, https://doi.org/10.1038/s43247-021-00328-y,
957   2021.

958   Ernle, L., Wang, N., Bekö, G., Morrison, G., Wargocki, P., J. Weschler, C., and Williams, J.: Assessment of aldehyde
959   contributions to PTR-MS m / z 69.07 in indoor air measurements, Environ. Sci. Atmospheres, 3, 1286–1295,
960   https://doi.org/10.1039/D3EA00055A, 2023.

961   Fall, R.: Abundant Oxygenates in the Atmosphere: A Biochemical Perspective, Chem. Rev., 103, 4941–4952,
962   https://doi.org/10.1021/cr0206521, 2003.

963   Fall, R., Karl, T., Hansel, A., Jordan, A., and Lindinger, W.: Volatile organic compounds emitted after leaf wounding:
964   On-line analysis by proton-transfer-reaction mass spectrometry, J. Geophys. Res. Atmospheres, 104, 15963–15974,
965   https://doi.org/10.1029/1999JD900144, 1999.

966   Fischer, E. V., Jacob, D. J., Yantosca, R. M., Sulprizio, M. P., Millet, D. B., Mao, J., Paulot, F., Singh, H. B., Roiger,
967   A., Ries, L., Talbot, R. W., Dzepina, K., and Pandey Deolal, S.: Atmospheric peroxyacetyl nitrate (PAN): a global
968   budget and source attribution, Atmospheric Chem. Phys., 14, 2679–2698, https://doi.org/10.5194/acp-14-2679-2014,
969   2014.

970   Fruekilde, P., Hjorth, J., Jensen, N. R., Kotzias, D., and Larsen, B.: OZONOLYSIS AT VEGETATION SURFACES:
971   A SOURCE OF ACETONE, 4-OXOPENTANAL, 6-METHYL-5-HEPTEN-2-ONE, AND GERANYL ACETONE
972   IN THE TROPOSPHERE, Atmos. Environ., Vol. 32, No. 11, 1893–1902, 1998.

973   Fuentes, J. D., Gerken, T., Chamecki, M., Stoy, P., Freire, L., and Ruiz-Plancarte, J.: Turbulent transport and reactions
974   of plant-emitted hydrocarbons in an Amazonian rain forest, Atmos. Environ., 279, 119094,
975   https://doi.org/10.1016/j.atmosenv.2022.119094, 2022.

976   Gouinguené, S. P. and Turlings, T. C. J.: The Effects of Abiotic Factors on Induced Volatile Emissions in Corn Plants,
977   Plant Physiol., 129, 1296–1307, https://doi.org/10.1104/pp.001941, 2002.

978   de Gouw, J. and Warneke, C.: Measurements of volatile organic compounds in the earth's atmosphere using proton-
979   transfer-reaction mass spectrometry, Mass Spectrom. Rev., 26, 223–257, https://doi.org/10.1002/mas.20119, 2007.

980   Guenther, A.: Natural emissions of non-methane volatile organic compounds, carbon monoxide, and oxides of
981   nitrogen from North America, Atmos. Environ., 34, 2205–2230, https://doi.org/10.1016/S1352-2310(99)00465-3,
982   2000.

983   Guenther, A.: Biological and Chemical Diversity of Biogenic Volatile Organic Emissions into the Atmosphere, Int.
984   Sch. Res. Not., 2013, e786290, https://doi.org/10.1155/2013/786290, 2013.

985   Guimbaud, C., Catoire, V., Bergeat, A., Michel, E., Schoon, N., Amelynck, C., Labonnette, D., and Poulet, G.:
986   Kinetics of the reactions of acetone and glyoxal with O2+ and NO+ ions and application to the detection of oxygenated
987   volatile organic compounds in the atmosphere by chemical ionization mass spectrometry, Int. J. Mass Spectrom., 263,
988   276–288, https://doi.org/10.1016/j.ijms.2007.03.006, 2007.

989   He, J., Halitschke, R., Schuman, M. C., and Baldwin, I. T.: Light dominates the diurnal emissions of herbivore-induced
990   volatiles in wild tobacco, BMC Plant Biol., 21, 401, https://doi.org/10.1186/s12870-021-03179-z, 2021.

991   Heiden, A. C., Kobel, K., Komenda, M., Koppmann, R., Shao, M., and Wildt, J.: Toluene emissions from plants,
992   Geophys. Res. Lett., 26, 1283–1286, https://doi.org/10.1029/1999GL900220, 1999.

993   Hellén, H., Hakola, H., Reissell, A., and Ruuskanen, T. M.: Carbonyl compounds in boreal coniferous forest air in
994   Hyytiälä, Southern Finland, Atmospheric Chem. Phys., 4, 1771–1780, https://doi.org/10.5194/acp-4-1771-2004,
995   2004.

996   Holanda, B. A., Pöhlker, M. L., Walter, D., Saturno, J., Sörgel, M., Ditas, J., Ditas, F., Schulz, C., Franco, M. A.,
997   Wang, Q., Donth, T., Artaxo, P., Barbosa, H. M. J., Borrmann, S., Braga, R., Brito, J., Cheng, Y., Dollner, M., Kaiser,
998   J. W., Klimach, T., Knote, C., Krüger, O. O., Fütterer, D., Lavrič, J. V., Ma, N., Machado, L. A. T., Ming, J., Morais,
999   F. G., Paulsen, H., Sauer, D., Schlager, H., Schneider, J., Su, H., Weinzierl, B., Walser, A., Wendisch, M., Ziereis, H.,
1000   Zöger, M., Pöschl, U., Andreae, M. O., and Pöhlker, C.: Influx of African biomass burning aerosol during the
1001   Amazonian dry season through layered transatlantic transport of black carbon-rich smoke, Atmospheric Chem. Phys.,
1002   20, 4757–4785, https://doi.org/10.5194/acp-20-4757-2020, 2020.

1003   Holanda, B. A., Franco, M. A., Walter, D., Artaxo, P., Carbone, S., Cheng, Y., Chowdhury, S., Ditas, F., Gysel-Beer,
1004   M., Klimach, T., Kremper, L. A., Krüger, O. O., Lavric, J. V., Lelieveld, J., Ma, C., Machado, L. A. T., Modini, R.
1005   L., Morais, F. G., Pozzer, A., Saturno, J., Su, H., Wendisch, M., Wolff, S., Pöhlker, M. L., Andreae, M. O., Pöschl,
1006   U., and Pöhlker, C.: African biomass burning affects aerosol cycling over the Amazon, Commun. Earth Environ., 4,
1007   1–15, https://doi.org/10.1038/s43247-023-00795-5, 2023.

1008   Holzinger, R., Sandoval-Soto, L., Rottenberger, S., Crutzen, P. J., and Kesselmeier, J.: Emissions of volatile organic
1009   compounds from Quercus ilex L. measured by Proton Transfer Reaction Mass Spectrometry under different
1010   environmental conditions, J. Geophys. Res. Atmospheres, 105, 20573–20579, https://doi.org/10.1029/2000JD900296,
1011   2000.

1012   Holzinger, R., Lee, A., Paw, K. T., and Goldstein, U. a. H.: Observations of oxidation products above a forest imply
1013   biogenic emissions of very reactive compounds, Atmospheric Chem. Phys., 5, 67–75, https://doi.org/10.5194/acp-5-
1014   67-2005, 2005.

1015   Hunter, E. P. L. and Lias, S. G.: Evaluated Gas Phase Basicities and Proton Affinities of Molecules: An Update, J.
1016   Phys. Chem. Ref. Data, 27, 413–656, https://doi.org/10.1063/1.556018, 1998.

1017   Isidorov, V. A., Zenkevich, I. G., and Ioffe, B. V.: Volatile organic compounds in the atmosphere of forests,
1018   Atmospheric Environ. 1967, 19, 1–8, https://doi.org/10.1016/0004-6981(85)90131-3, 1985.

Jacob, D. J., Field, B. D., Jin, E. M., Bey, I., Li, Q., Logan, J. A., Yantosca, R. M., and Singh, H. B.: Atmospheric budget of acetone, J. Geophys. Res. Atmospheres, 107, ACH 5-1-ACH 5-17, https://doi.org/10.1029/2001JD000694, 2002.

Jan, R., Asaf, S., Numan, M., Lubna, and Kim, K.-M.: Plant Secondary Metabolite Biosynthesis and Transcriptional Regulation in Response to Biotic and Abiotic Stress Conditions, Agronomy, 11, 968, https://doi.org/10.3390/agronomy11050968, 2021.

Jardine, K., Barron-Gafford, G. A., Norman, J. P., Abrell, L., Monson, R. K., Meyers, K. T., Pavao-Zuckerman, M., Dontsova, K., Kleist, E., Werner, C., and Huxman, T. E.: Green leaf volatiles and oxygenated metabolite emission bursts from mesquite branches following light–dark transitions, Photosynth. Res., 113, 321–333, https://doi.org/10.1007/s11120-012-9746-5, 2012a.

Jardine, K. J., Monson, R. K., Abrell, L., Saleska, S. R., Arneth, A., Jardine, A., Ishida, F. Y., Serrano, A. M. Y., Artaxo, P., Karl, T., Fares, S., Goldstein, A., Loreto, F., and Huxman, T.: Within-plant isoprene oxidation confirmed by direct emissions of oxidation products methyl vinyl ketone and methacrolein, Glob. Change Biol., 18, 973–984, https://doi.org/10.1111/j.1365-2486.2011.02610.x, 2012b.

Jardine, K. J., Meyers, K., Abrell, L., Alves, E. G., Yanez Serrano, A. M., Kesselmeier, J., Karl, T., Guenther, A., Vickers, C., and Chambers, J. Q.: Emissions of putative isoprene oxidation products from mango branches under abiotic stress, J. Exp. Bot., 64, 3669–3679, https://doi.org/10.1093/jxb/ert202, 2013.

Jardine, K. J., Chambers, J. Q., Holm, J., Jardine, A. B., Fontes, C. G., Zorzanelli, R. F., Meyers, K. T., De Souza, V. F., Garcia, S., Gimenez, B. O., Piva, L. R. de O., Higuchi, N., Artaxo, P., Martin, S., and Manzi, A. O.: Green Leaf Volatile Emissions during High Temperature and Drought Stress in a Central Amazon Rainforest, Plants, 4, 678–690, https://doi.org/10.3390/plants4030678, 2015.

Jiménez, E., Lanza, B., Martínez, E., and Albaladejo, J.: Daytime tropospheric loss of hexanal and <I>trans</I>-2-hexenal: OH kinetics and UV photolysis, Atmospheric Chem. Phys., 7, 1565–1574, https://doi.org/10.5194/acp-7-1565-2007, 2007.

Jordan, A., Haidacher, S., Hanel, G., Hartungen, E., Märk, L., Seehauser, H., Schottkowsky, R., Sulzer, P., and Märk, T. D.: A high resolution and high sensitivity proton-transfer-reaction time-of-flight mass spectrometer (PTR-TOF-MS), Int. J. Mass Spectrom., 286, 122–128, https://doi.org/10.1016/j.ijms.2009.07.005, 2009.

Jordi Vilà-Guerau de Arellano, C. C. van H., Bart J. H. van Stratum, and Kees van den Dries: Atmospheric Boundary Layer, Cambridge University Press, 2015.

Kalalian, C., Abis, L., Depoorter, A., Lunardelli, B., Perrier, S., and George, C.: Influence of indoor chemistry on the emission of mVOCs from Aspergillus niger molds, Sci. Total Environ., 741, 140148, https://doi.org/10.1016/j.scitotenv.2020.140148, 2020.

Karl, T., Guenther, A., Spirig, C., Hansel, A., and Fall, R.: Seasonal variation of biogenic VOC emissions above a mixed hardwood forest in northern Michigan, Geophys. Res. Lett., 30, https://doi.org/10.1029/2003GL018432, 2003.

Karl, T., Potosnak, M., Guenther, A., Clark, D., Walker, J., Herrick, J. D., and Geron, C.: Exchange processes of volatile organic compounds above a tropical rain forest: Implications for modeling tropospheric chemistry above dense vegetation, J. Geophys. Res. Atmospheres, 109, https://doi.org/10.1029/2004JD004738, 2004.

Karl, T., Hansel, A., Cappellin, L., Kaser, L., Herdlinger-Blatt, I., and Jud, W.: Selective measurements of isoprene and 2-methyl-3-buten-2-ol based on NO⁺ ionization mass spectrometry, Atmospheric Chem. Phys., 12, 11877–11884, https://doi.org/10.5194/acp-12-11877-2012, 2012.

1059   Kesselmeier, J.: Exchange of Short-Chain Oxygenated Volatile Organic Compounds (VOCs) between Plants and the
1060   Atmosphere: A Compilation of Field and Laboratory Studies, J. Atmospheric Chem., 39, 219–233,
1061   https://doi.org/10.1023/A:1010632302076, 2001.

1062   Kesselmeier, J. and Staudt, M.: Biogenic Volatile Organic Compounds (VOC): An Overview on Emission, Physiology
1063   and Ecology, J. Atmospheric Chem., 33, 23–88, https://doi.org/10.1023/A:1006127516791, 1999.

1064   Kesselmeier, J., Bode, K., Hofmann, U., Müller, H., Schäfer, L., Wolf, A., Ciccioli, P., Brancaleoni, E., Cecinato, A.,
1065   Frattoni, M., Foster, P., Ferrari, C., Jacob, V., Fugit, J. L., Dutaur, L., Simon, V., and Torres, L.: Emission of short
1066   chained organic acids, aldehydes and monoterpenes from Quercus ilex L. and Pinus pinea L. in relation to
1067   physiological activities, carbon budget and emission algorithms, Atmos. Environ., 31, 119–133,
1068   https://doi.org/10.1016/S1352-2310(97)00079-4, 1997.

1069   Kesselmeier, J., Kuhn, U., Wolf, A., Andreae, M. O., Ciccioli, P., Brancaleoni, E., Frattoni, M., Guenther, A.,
1070   Greenberg, J., De Castro Vasconcellos, P., de Oliva, T., Tavares, T., and Artaxo, P.: Atmospheric volatile organic
1071   compounds (VOC) at a remote tropical forest site in central Amazonia, Atmos. Environ., 34, 4063–4072,
1072   https://doi.org/10.1016/S1352-2310(00)00186-2, 2000.

1073   Khan, M. A. H., Cooke, M. C., Utembe, S. R., Archibald, A. T., Derwent, R. G., Xiao, P., Percival, C. J., Jenkin, M.
1074   E., Morris, W. C., and Shallcross, D. E.: Global modeling of the nitrate radical (NO3) for present and pre-industrial
1075   scenarios, Atmospheric Res., 164–165, 347–357, https://doi.org/10.1016/j.atmosres.2015.06.006, 2015.

1076   Kirstine, W., Galbally, I., Ye, Y., and Hooper, M.: Emissions of volatile organic compounds (primarily oxygenated
1077   species) from pasture, J. Geophys. Res. Atmospheres, 103, 10605–10619, https://doi.org/10.1029/97JD03753, 1998.

1078   Kirstine, W. V. and Galbally, I. E.: The global atmospheric budget of ethanol revisited, Atmospheric Chem. Phys.,
1079   12, 545–555, https://doi.org/10.5194/acp-12-545-2012, 2012.

1080   König, G., Brunda, M., Puxbaum, H., Hewitt, C. N., Duckham, S. C., and Rudolph, J.: Relative contribution of
1081   oxygenated hydrocarbons to the total biogenic VOC emissions of selected mid-European agricultural and natural plant
1082   species, Atmos. Environ., 29, 861–874, https://doi.org/10.1016/1352-2310(95)00026-U, 1995.

1083   Koss, A. R., Warneke, C., Yuan, B., Coggon, M. M., Veres, P. R., and de Gouw, J. A.: Evaluation of
1084   NO⁺ reagent ion chemistry for online measurements ofatmospheric volatile organic
1085   compounds, Atmospheric Meas. Tech., 9, 2909–2925, https://doi.org/10.5194/amt-9-2909-2016, 2016.

1086   Kreuzwieser, J., Kühnemann, F., Martis, A., Rennenberg, H., and Urban, W.: Diurnal pattern of acetaldehyde emission
1087   by flooded poplar trees, Physiol. Plant., 108, 79–86, https://doi.org/10.1034/j.1399-3054.2000.108001079.x, 2000.

1088   Kuhn, U., Rottenberger, S., Biesenthal, T., Wolf, A., Schebeske, G., Ciccioli, P., Brancaleoni, E., Frattoni, M.,
1089   Tavares, T. M., and Kesselmeier, J.: Seasonal differences in isoprene and light-dependent monoterpene emission by
1090   Amazonian tree species, Glob. Change Biol., 10, 663–682, https://doi.org/10.1111/j.1529-8817.2003.00771.x, 2004a.

1091   Kuhn, U., Rottenberger, S., Biesenthal, T., Wolf, A., Schebeske, G., Ciccioli, P., and Kesselmeier, J.: Strong
1092   correlation between isoprene emission and gross photosynthetic capacity during leaf phenology of the tropical tree
1093   species Hymenaea courbaril with fundamental changes in volatile organic compounds emission composition during
1094   early leaf development, Plant Cell Environ., 27, 1469–1485, https://doi.org/10.1111/j.1365-3040.2004.01252.x,
1095   2004b.

1096   Kuhn, U., Andreae, M. O., Ammann, C., Araújo, A. C., Brancaleoni, E., Ciccioli, P., Dindorf, T., Frattoni, M., Gatti,
1097   L. V., Ganzeveld, L., Kruijt, B., Lelieveld, J., Lloyd, J., Meixner, F. X., Nobre, A. D., Pöschl, U., Spirig, C., Stefani,
1098   P., Thielmann, A., Valentini, R., and Kesselmeier, J.: Isoprene and monoterpene fluxes from Central Amazonian
1099   rainforest inferred from tower-based and airborne measurements, and implications on the atmospheric chemistry and
1100   the local carbon budget, Atmospheric Chem. Phys., 7, 2855–2879, https://doi.org/10.5194/acp-7-2855-2007, 2007.

1101 Ladino-Orjuela, G., Gomes, E., da Silva, R., Salt, C., and Parsons, J. R.: Metabolic Pathways for Degradation of
1102 Aromatic Hydrocarbons by Bacteria, in: Reviews of Environmental Contamination and Toxicology Volume 237, vol.
1103 237, edited by: de Voogt, W. P., Springer International Publishing, Cham, 105–121, https://doi.org/10.1007/978-3-
1104 319-23573-8_5, 2016.

1105 Langford, B., Misztal, P. K., Nemitz, E., Davison, B., Helfter, C., Pugh, T. a. M., MacKenzie, A. R., Lim, S. F., and
1106 Hewitt, C. N.: Fluxes and concentrations of volatile organic compounds from a South-East Asian tropical rainforest,
1107 Atmospheric Chem. Phys., 10, 8391–8412, https://doi.org/10.5194/acp-10-8391-2010, 2010.

1108 Laothawornkitkul, J., Taylor, J. E., Paul, N. D., and Hewitt, C. N.: Biogenic volatile organic compounds in the Earth
1109 system, New Phytol., 183, 27–51, https://doi.org/10.1111/j.1469-8137.2009.02859.x, 2009.

1110 Lary, D. J. and Shallcross, D. E.: Central role of carbonyl compounds in atmospheric chemistry, J. Geophys. Res.
1111 Atmospheres, 105, 19771–19778, https://doi.org/10.1029/1999JD901184, 2000.

1112 Lelieveld, J., Gromov, S., Pozzer, A., and Taraborrelli, D.: Global tropospheric hydroxyl distribution, budget and
1113 reactivity, Atmospheric Chem. Phys., 16, 12477–12493, https://doi.org/10.5194/acp-16-12477-2016, 2016.

1114 Lewis, H. L.: Caproic Acid Metabolism and the Production of 2-Pentanone and Gluconic Acid by Aspergillus niger,
1115 Microbiology, 63, 203–210, https://doi.org/10.1099/00221287-63-2-203, 1970.

1116 Li, X.-B., Zhang, C., Liu, A., Yuan, B., Yang, H., Liu, C., Wang, S., Huangfu, Y., Qi, J., Liu, Z., He, X., Song, X.,
1117 Chen, Y., Peng, Y., Zhang, X., Zheng, E., Yang, L., Yang, Q., Qin, G., Zhou, J., and Shao, M.: Assessment of long
1118 tubing in measuring atmospheric trace gases: applications on tall towers, Environ. Sci. Atmospheres, 3, 506–520,
1119 https://doi.org/10.1039/D2EA00110A, 2023.

1120 Liu, Q., Gao, Y., Huang, W., Ling, Z., Wang, Z., and Wang, X.: Carbonyl compounds in the atmosphere: A review
1121 of abundance, source and their contributions to O3 and SOA formation, Atmospheric Res., 274, 106184,
1122 https://doi.org/10.1016/j.atmosres.2022.106184, 2022.

1123 Liu, Y., Brito, J., Dorris, M. R., Rivera-Rios, J. C., Seco, R., Bates, K. H., Artaxo, P., Duvoisin, S., Keutsch, F. N.,
1124 Kim, S., Goldstein, A. H., Guenther, A. B., Manzi, A. O., Souza, R. A. F., Springston, S. R., Watson, T. B., McKinney,
1125 K. A., and Martin, S. T.: Isoprene photochemistry over the Amazon rainforest, Proc. Natl. Acad. Sci., 113, 6125–
1126 6130, https://doi.org/10.1073/pnas.1524136113, 2016.

1127 Matsui, K., Sugimoto, K., Kakumyan, P., Khorobrykh, S. A., and Mano, J.: Volatile Oxylipins and Related
1128 Compounds Formed Under Stress in Plants, in: Lipidomics: Volume 2: Methods and Protocols, edited by: Armstrong,
1129 D., Humana Press, Totowa, NJ, 17–28, https://doi.org/10.1007/978-1-60761-325-1_2, 2010.

1130 Mellouki, A., Wallington, T. J., and Chen, J.: Atmospheric Chemistry of Oxygenated Volatile Organic Compounds:
1131 Impacts on Air Quality and Climate, Chem. Rev., 115, 3984–4014, https://doi.org/10.1021/cr500549n, 2015.

1132 Mumm, R. and Dicke, M.: Variation in natural plant products and the attraction of bodyguards involved in indirect
1133 plant defense, Can. J. Zool., 88, 628–667, https://doi.org/10.1139/Z10-032, 2010.

1134 Nguyen, T. B., Crounse, J. D., Teng, A. P., St. Clair, J. M., Paulot, F., Wolfe, G. M., and Wennberg, P. O.: Rapid
1135 deposition of oxidized biogenic compounds to a temperate forest, Proc. Natl. Acad. Sci., 112, E392–E401,
1136 https://doi.org/10.1073/pnas.1418702112, 2015.

1137 Niinemets, Ü., Fares, S., Harley, P., and Jardine, K. J.: Bidirectional exchange of biogenic volatiles with vegetation:
1138 emission sources, reactions, breakdown and deposition, Plant Cell Environ., 37, 1790–1809,
1139 https://doi.org/10.1111/pce.12322, 2014.

1140   Orzechowska, G. E., Nguyen, H. T., and Paulson, S. E.: Photochemical Sources of Organic Acids. 2. Formation of
1141   C5−C9 Carboxylic Acids from Alkene Ozonolysis under Dry and Humid Conditions, J. Phys. Chem. A, 109, 5366–
1142   5375, https://doi.org/10.1021/jp050167k, 2005.

1143   Pagonis, D., Krechmer, J. E., de Gouw, J., Jimenez, J. L., and Ziemann, P. J.: Effects of gas–wall partitioning in Teflon
1144   tubing and instrumentation on time-resolved measurements of gas-phase organic compounds, Atmospheric Meas.
1145   Tech., 10, 4687–4696, https://doi.org/10.5194/amt-10-4687-2017, 2017.

1146   Parolin, P., De Simone, O., Haase, K., Waldhoff, D., Rottenberger, S., Kuhn, U., Kesselmeier, J., Kleiss, B., Schmidt,
1147   W., Pledade, M. T. F., and Junk, W. J.: Central Amazonian floodplain forests: Tree adaptations in a pulsing system,
1148   Bot. Rev., 70, 357–380, https://doi.org/10.1663/0006-8101(2004)070[0357:CAFFTA]2.0.CO;2, 2004.

1149   Pfannerstill, E. Y., Reijrink, N. G., Edtbauer, A., Ringsdorf, A., Zannoni, N., Araújo, A., Ditas, F., Holanda, B. A.,
1150   Sá, M. O., Tsokankunku, A., Walter, D., Wolff, S., Lavrič, J. V., Pöhlker, C., Sörgel, M., and Williams, J.: Total OH
1151   reactivity over the Amazon rainforest: variability with temperature, wind, rain, altitude, time of day, season, and an
1152   overall budget closure, Atmospheric Chem. Phys., 21, 6231–6256, https://doi.org/10.5194/acp-21-6231-2021, 2021.

1153   Pöhlker, C., Walter, D., Paulsen, H., Könemann, T., Rodríguez-Caballero, E., Moran-Zuloaga, D., Brito, J., Carbone,
1154   S., Degrendele, C., Després, V. R., Ditas, F., Holanda, B. A., Kaiser, J. W., Lammel, G., Lavrič, J. V., Jing, M.,
1155   Pickersgill, D., Pöhlker, M. L., Praß, M., Löbs, N., Saturno, J., Sörgel, M., Wang, Q., Weber, B., Wolff, S., Artaxo,
1156   P., Pöschl, U., and Andreae, M. O.: Land cover and its transformation in the backward trajectory footprint region of
1157   the Amazon Tall Tower Observatory, Atmospheric Chem. Phys., 19, 8425–8470, https://doi.org/10.5194/acp-19-
1158   8425-2019, 2019.

1159   Prather, M. J. and Jacob, D. J.: A persistent imbalance in HOx and NOx photochemistry of the upper troposphere
1160   driven by deep tropical convection, Geophys. Res. Lett., 24, 3189–3192, https://doi.org/10.1029/97GL03027, 1997.

1161   Restrepo-Coupe, N., da Rocha, H. R., Hutyra, L. R., da Araujo, A. C., Borma, L. S., Christoffersen, B., Cabral, O. M.
1162   R., de Camargo, P. B., Cardoso, F. L., da Costa, A. C. L., Fitzjarrald, D. R., Goulden, M. L., Kruijt, B., Maia, J. M.
1163   F., Malhi, Y. S., Manzi, A. O., Miller, S. D., Nobre, A. D., von Randow, C., Sá, L. D. A., Sakai, R. K., Tota, J., Wofsy,
1164   S. C., Zanchi, F. B., and Saleska, S. R.: What drives the seasonality of photosynthesis across the Amazon basin? A
1165   cross-site analysis of eddy flux tower measurements from the Brasil flux network, Agric. For. Meteorol., 182–183,
1166   128–144, https://doi.org/10.1016/j.agrformet.2013.04.031, 2013.

1167   Ringsdorf, A., Edtbauer, A., Vilà-Guerau de Arellano, J., Pfannerstill, E. Y., Gromov, S., Kumar, V., Pozzer, A.,
1168   Wolff, S., Tsokankunku, A., Soergel, M., Sá, M. O., Araújo, A., Ditas, F., Poehlker, C., Lelieveld, J., and Williams,
1169   J.: Inferring the diurnal variability of OH radical concentrations over the Amazon from BVOC measurements, Sci.
1170   Rep., 13, 14900, https://doi.org/10.1038/s41598-023-41748-4, 2023.

1171   Rivera-Rios, J. C., Nguyen, T. B., Crounse, J. D., Jud, W., St. Clair, J. M., Mikoviny, T., Gilman, J. B., Lerner, B. M.,
1172   Kaiser, J. B., Gouw, J., Wisthaler, A., Hansel, A., Wennberg, P. O., Seinfeld, J. H., and Keutsch, F. N.: Conversion
1173   of hydroperoxides to carbonyls in field and laboratory instrumentation: Observational bias in diagnosing pristine
1174   versus anthropogenically controlled atmospheric chemistry, Geophys. Res. Lett., 41, 8645–8651,
1175   https://doi.org/10.1002/2014GL061919, 2014.

1176   Roberts, J. M: PAN and Related Compounds, in: Volatile Organic Compounds in the Atmosphere, Blackwell
1177   Publishing Ltd, 2007.

1178   Romano, A. and Hanna, G. B.: Identification and quantification of VOCs by proton transfer reaction time of flight
1179   mass spectrometry: An experimental workflow for the optimization of specificity, sensitivity, and accuracy, J. Mass
1180   Spectrom., 53, 287–295, https://doi.org/10.1002/jms.4063, 2018.

1181   Rottenberger, S., Kuhn, U., Wolf, A., Schebeske, G., Oliva, S. T., Tavares, T. M., and Kesselmeier, J.: Exchange of
1182   Short-Chain Aldehydes Between Amazonian Vegetation and the Atmosphere, Ecol. Appl., 14, 247–262,
1183   https://doi.org/10.1890/01-6027, 2004.

Rottenberger, S., Kleiss, B., Kuhn, U., Wolf, A., Piedade, M. T. F., Junk, W., and Kesselmeier, J.: The effect of flooding on the exchange of the volatile C_2-compounds ethanol, acetaldehyde and acetic acid between leaves of Amazonian floodplain tree species and the atmosphere, Biogeosciences, 5, 1085–1100, https://doi.org/10.5194/bg-5-1085-2008, 2008.

Rummel, U., Ammann, C., Gut, A., Meixner, F. X., and Andreae, M. O.: Eddy covariance measurements of nitric oxide flux within an Amazonian rain forest, J. Geophys. Res. Atmospheres, 107, LBA 17-1-LBA 17-9, https://doi.org/10.1029/2001JD000520, 2002.

Scala, A., Allmann, S., Mirabella, R., Haring, M. A., and Schuurink, R. C.: Green Leaf Volatiles: A Plant's Multifunctional Weapon against Herbivores and Pathogens, Int. J. Mol. Sci., 14, 17781–17811, https://doi.org/10.3390/ijms140917781, 2013.

Schade, G. W. and Goldstein, A. H.: Fluxes of oxygenated volatile organic compounds from a ponderosa pine plantation, J. Geophys. Res. Atmospheres, 106, 3111–3123, https://doi.org/10.1029/2000JD900592, 2001.

Sebbar, N., Bozzelli, J. W., and Bockhorn, H.: Thermochemistry and Reaction Paths in the Oxidation Reaction of Benzoyl Radical: C6H5C•(=O), J. Phys. Chem. A, 115, 11897–11914, https://doi.org/10.1021/jp2078067, 2011.

Seco, R., Peñuelas, J., and Filella, I.: Short-chain oxygenated VOCs: Emission and uptake by plants and atmospheric sources, sinks, and concentrations, Atmos. Environ., 41, 2477–2499, https://doi.org/10.1016/j.atmosenv.2006.11.029, 2007.

Singh, H. B., Herlth, D., O'Hara, D., Salas, L., Torres, A. L., Gregory, G. L., Sachse, G. W., and Kasting, J. F.: Atmospheric peroxyacetyl nitrate measurements over the Brazilian Amazon Basin during the wet season: Relationships with nitrogen oxides and ozone, J. Geophys. Res. Atmospheres, 95, 16945–16954, https://doi.org/10.1029/JD095iD10p16945, 1990.

Singh, H. B., Salas, L. J., Chatfield, R. B., Czech, E., Fried, A., Walega, J., Evans, M. J., Field, B. D., Jacob, D. J., Blake, D., Heikes, B., Talbot, R., Sachse, G., Crawford, J. H., Avery, M. A., Sandholm, S., and Fuelberg, H.: Analysis of the atmospheric distribution, sources, and sinks of oxygenated volatile organic chemicals based on measurements over the Pacific during TRACE-P, J. Geophys. Res. Atmospheres, 109, https://doi.org/10.1029/2003JD003883, 2004.

Smith, D., Wang, T., and Španěl, P.: Analysis of ketones by selected ion flow tube mass spectrometry, Rapid Commun. Mass Spectrom., 17, 2655–2660, https://doi.org/10.1002/rcm.1244, 2003.

Smith, D., Chippendale, T. W. E., and Španěl, P.: Selected ion flow tube, SIFT, studies of the reactions of H3O+, NO+ and O2+ with some biologically active isobaric compounds in preparation for SIFT-MS analyses, Int. J. Mass Spectrom., 303, 81–89, https://doi.org/10.1016/j.ijms.2011.01.005, 2011.

Španěl, P. and Smith, D.: SIFT studies of the reactions of H3O+, NO+ and O+2 with a series of volatile carboxylic acids and esters, Int. J. Mass Spectrom. Ion Process., 172, 137–147, https://doi.org/10.1016/S0168-1176(97)00246-2, 1998.

Španěl, P. and Smith, D.: SIFT studies of the reactions of H3O+, NO+ and O2+ with several ethers, Int. J. Mass Spectrom. Ion Process., 172, 239–247, https://doi.org/10.1016/S0168-1176(97)00277-2, 1998.

Španěl, P., Ji, Y., and Smith, D.: SIFT studies of the reactions of H3O+, NO+ and O2+ with a series of aldehydes and ketones, Int. J. Mass Spectrom. Ion Process., 165–166, 25–37, https://doi.org/10.1016/S0168-1176(97)00166-3, 1997.

Španěl, P., Wang, T., and Smith, D.: A selected ion flow tube, SIFT, study of the reactions of H3O+, NO+ and O2+ ions with a series of diols, Int. J. Mass Spectrom., 218, 227–236, https://doi.org/10.1016/S1387-3806(02)00724-8, 2002.

1224 Tani, A. and Hewitt, C. N.: Uptake of Aldehydes and Ketones at Typical Indoor Concentrations by Houseplants,
1225 Environ. Sci. Technol., 43, 8338–8343, https://doi.org/10.1021/es9020316, 2009.

1226 Tani, A., Tobe, S., and Shimizu, S.: Uptake of Methacrolein and Methyl Vinyl Ketone by Tree Saplings and
1227 Implications for Forest Atmosphere, Environ. Sci. Technol., 44, 7096–7101, https://doi.org/10.1021/es1017569, 2010.

1228 Tani, A., Tobe, S., and Shimizu, S.: Leaf uptake of methyl ethyl ketone and croton aldehyde by *Castanopsis sieboldii*
1229 and *Viburnum odoratissimum* saplings, Atmos. Environ., 70, 300–306,
1230 https://doi.org/10.1016/j.atmosenv.2012.12.043, 2013.

1231 Trebs, I., Mayol-Bracero, O. L., Pauliquevis, T., Kuhn, U., Sander, R., Ganzeveld, L., Meixner, F. X., Kesselmeier,
1232 J., Artaxo, P., and Andreae, M. O.: Impact of the Manaus urban plume on trace gas mixing ratios near the surface in
1233 the Amazon Basin: Implications for the NO-NO2-O3 photostationary state and peroxy radical levels, J. Geophys. Res.
1234 Atmospheres, 117, https://doi.org/10.1029/2011JD016386, 2012.

1235 Villanueva, F., Tapia, A., Notario, A., Albaladejo, J., and Martínez, E.: Ambient levels and temporal trends of VOCs,
1236 including carbonyl compounds, and ozone at Cabañeros National Park border, Spain, Atmos. Environ., 85, 256–265,
1237 https://doi.org/10.1016/j.atmosenv.2013.12.015, 2014.

1238 Villanueva-Fierro, I., Popp, C. J., and Martin, R. S.: Biogenic emissions and ambient concentrations of hydrocarbons,
1239 carbonyl compounds and organic acids from ponderosa pine and cottonwood trees at rural and forested sites in Central
1240 New Mexico, Atmos. Environ., 38, 249–260, https://doi.org/10.1016/j.atmosenv.2003.09.051, 2004.

1241 Wang, C., Yuan, B., Wu, C., Wang, S., Qi, J., Wang, B., Wang, Z., Hu, W., Chen, W., Ye, C., Wang, W., Sun, Y.,
1242 Wang, C., Huang, S., Song, W., Wang, X., Yang, S., Zhang, S., Xu, W., Ma, N., Zhang, Z., Jiang, B., Su, H., Cheng,
1243 Y., Wang, X., and Shao, M.: Measurements of higher alkanes using NO⁺ chemical ionization
1244 in PTR-ToF-MS: important contributions of higher alkanes to secondary organic aerosols in China, Atmospheric
1245 Chem. Phys., 20, 14123–14138, https://doi.org/10.5194/acp-20-14123-2020, 2020a.

1246 Wang, M., Zhang, L., Boo, K. H., Park, E., Drakakaki, G., and Zakharov, F.: PDC1, a pyruvate/α-ketoacid
1247 decarboxylase, is involved in acetaldehyde, propanal and pentanal biosynthesis in melon (Cucumis melo L.) fruit,
1248 Plant J., 98, 112–125, https://doi.org/10.1111/tpj.14204, 2019.

1249 Wang, N., Edtbauer, A., Stönner, C., Pozzer, A., Bourtsoukidis, E., Ernle, L., Dienhart, D., Hottmann, B., Fischer, H.,
1250 Schuladen, J., Crowley, J. N., Paris, J.-D., Lelieveld, J., and Williams, J.: Measurements of carbonyl compounds
1251 around the Arabian Peninsula indicate large missing sources of acetaldehyde, Gases/Field
1252 Measurements/Troposphere/Chemistry (chemical composition and reactions), https://doi.org/10.5194/acp-2020-135,
1253 2020b.

1254 Warneck, P.; Williams, J.: The Atmospheric Chemists Companion, 1., Springer Verlag GmbH, 2012.

1255 Warneke, C., Karl, T., Judmaier, H., Hansel, A., Jordan, A., Lindinger, W., and Crutzen, P. J.: Acetone, methanol,
1256 and other partially oxidized volatile organic emissions from dead plant matter by abiological processes: Significance
1257 for atmospheric HOx chemistry, Glob. Biogeochem. Cycles, 13, 9–17, https://doi.org/10.1029/98GB02428, 1999.

1258 Williams, J., Fischer, H., Harris, G. W., Crutzen, P. J., Hoor, P., Hansel, A., Holzinger, R., Warneke, C., Lindinger,
1259 W., Scheeren, B., and Lelieveld, J.: Variability-lifetime relationship for organic trace gases: A novel aid to compound
1260 identification and estimation of HO concentrations, J. Geophys. Res. Atmospheres, 105, 20473–20486,
1261 https://doi.org/10.1029/2000JD900203, 2000.

1262 Williams, J., Pöschl, U., Crutzen, P. J., Hansel, A., Holzinger, R., Warneke, C., Lindinger, W., and Lelieveld, J.: An
1263 Atmospheric Chemistry Interpretation of Mass Scans Obtained from a Proton Transfer Mass Spectrometer Flown over
1264 the Tropical Rainforest of Surinam, 2001.

1265 Wolfe, G. M., Thornton, J. A., McKay, M., and Goldstein, A. H.: Forest-atmosphere exchange of ozone: sensitivity
1266 to very reactive biogenic VOC emissions and implications for in-canopy photochemistry, Atmospheric Chem. Phys.,
1267 11, 7875–7891, https://doi.org/10.5194/acp-11-7875-2011, 2011.

1268 Xing, J.-H., Ono, M., Kuroda, A., Obi, K., Sato, K., and Imamura, T.: Kinetic Study of the Daytime Atmospheric Fate
1269 of (Z)-3-Hexenal, J. Phys. Chem. A, 116, 8523–8529, https://doi.org/10.1021/jp303202h, 2012.

1270 Yamauchi, Y., Kunishima, M., Mizutani, M., and Sugimoto, Y.: Reactive short-chain leaf volatiles act as powerful
1271 inducers of abiotic stress-related gene expression, Sci. Rep., 5, 8030, https://doi.org/10.1038/srep08030, 2015.

1272 Yáñez-Serrano, A. M., Nölscher, A. C., Williams, J., Wolff, S., Alves, E., Martins, G. A., Bourtsoukidis, E., Brito, J.,
1273 Jardine, K., Artaxo, P., and Kesselmeier, J.: Diel and seasonal changes of biogenic volatile organic compounds within
1274 and above an Amazonian rainforest, Atmospheric Chem. Phys., 15, 3359–3378, https://doi.org/10.5194/acp-15-3359-
1275 2015, 2015.

1276 Yáñez-Serrano, A. M., Nölscher, A. C., Bourtsoukidis, E., Derstroff, B., Zannoni, N., Gros, V., Lanza, M., Brito, J.,
1277 Noe, S. M., House, E., Hewitt, C. N., Langford, B., Nemitz, E., Behrendt, T., Williams, J., Artaxo, P., Andreae, M.
1278 O., and Kesselmeier, J.: Atmospheric mixing ratios of methyl ethyl ketone (2-butanone) in tropical, boreal, temperate
1279 and marine environments, Atmospheric Chem. Phys., 16, 10965–10984, https://doi.org/10.5194/acp-16-10965-2016,
1280 2016.

1281 Yee, L. D., Isaacman-VanWertz, G., Wernis, R. A., Meng, M., Rivera, V., Kreisberg, N. M., Hering, S. V., Bering,
1282 M. S., Glasius, M., Upshur, M. A., Gray Bé, A., Thomson, R. J., Geiger, F. M., Offenberg, J. H., Lewandowski, M.,
1283 Kourtchev, I., Kalberer, M., de Sá, S., Martin, S. T., Alexander, M. L., Palm, B. B., Hu, W., Campuzano-Jost, P., Day,
1284 D. A., Jimenez, J. L., Liu, Y., McKinney, K. A., Artaxo, P., Viegas, J., Manzi, A., Oliveira, M. B., de Souza, R.,
1285 Machado, L. A. T., Longo, K., and Goldstein, A. H.: Observations of sesquiterpenes and their oxidation products in
1286 central Amazonia during the wet and dry seasons, Atmospheric Chem. Phys., 18, 10433–10457,
1287 https://doi.org/10.5194/acp-18-10433-2018, 2018.

1288 Yee, L. D., Goldstein, A. H., and Kreisberg, N. M.: Investigating Secondary Aerosol Processes in the Amazon through
1289 Molecular-level Characterization of Semi-Volatile Organics, Univ. of California, Berkeley, CA (United States),
1290 https://doi.org/10.2172/1673764, 2020.

1291 Zannoni, N., Wikelski, M., Gagliardo, A., Raza, A., Kramer, S., Seghetti, C., Wang, N., Edtbauer, A., and Williams,
1292 J.: Identifying volatile organic compounds used for olfactory navigation by homing pigeons, Sci. Rep., 10, 15879,
1293 https://doi.org/10.1038/s41598-020-72525-2, 2020a.

1294 Zannoni, N., Leppla, D., Lembo Silveira de Assis, P. I., Hoffmann, T., Sá, M., Araújo, A., and Williams, J.: Surprising
1295 chiral composition changes over the Amazon rainforest with height, time and season, Commun. Earth Environ., 1, 1–
1296 11, https://doi.org/10.1038/s43247-020-0007-9, 2020b.

1297